14. Liu HD, Li W, Chen ZR, Hu YC, Zhang DD, Shen W, et al. Expression of the NLRP3 inflammasome in cerebral cortex after traumatic brain injury in a rat model. *Neurochem Res*. 2013; **38**: 2072–83.
15. Heneka MT, Kummer MP, Stutz A, Delekate A, Schwartz S, Vieira-Saecker A, et al. NLRP3 is activated in Alzheimer's disease and contributes to pathology in APP/PS1 mice. *Nature*. 2013; **493**: 674–8.
16. Lequerré T, Vittecoq O, Saugier-Veber P, Goldenberg A, Patoz P, Frébourg T, et al. A cryopyrin-associated periodic syndrome with joint destruction. *Rheumatology (Oxford)*. 2007; **46**: 709–14.
17. Compeyrot-Lacassagne S, Tran TA, Guillaume-Czitrom S, Marie I, Koné-Paut I. Brain multiple sclerosis-like lesions in a patient with Muckle-Wells syndrome. *Rheumatology (Oxford)*. 2009; **48**: 1618–9.
18. Ming X, Li W, Maeda Y, Blumberg B, Raval S, Cook SD, et al. Caspase-1 expression in multiple sclerosis plaques and cultured glial cells. *J Neurol Sci*. 2002; **197**: 9–18.
19. Jha S, Srivastava SY, Brickey WJ, Iocca H, Toews A, Morrison JP, et al. The inflammasome sensor, NLRP3, regulates CNS inflammation and demyelination via caspase-1 and interleukin-18. *J Neurosci*. 2010; **30**: 15811–20.
20. Gris D, Ye Z, Iocca HA, Wen H, Craven RR, Gris P, et al. NLRP3 plays a critical role in the development of experimental autoimmune encephalomyelitis by mediating Th1 and Th17 responses. *J Immunol*. 2010; **185**: 974–81.
21. Inoue M, Shinohara ML. The role of interferon-β in the treatment of multiple sclerosis and experimental autoimmune encephalomyelitis – in the perspective of inflammasomes. *Immunology*. 2013; **139**: 11–8.
22. Guarda G, Braun M, Staehli F, Tardivel A, Mattmann C, Förster I, et al. Type I interferon inhibits interleukin-1 production and inflammasome activation. *Immunity*. 2011; **34**: 213–23.
23. Satoh J, Obayashi S, Misawa T, Tabunoki H, Yamamura T, Arima K, et al. Neuromyelitis optica/Devic's disease: gene expression profiling of brain lesions. *Neuropathology*. 2008; **28**: 561–76.
24. Satoh J, Tabunoki H, Ishida T, Saito Y, Konno H, Arima K. Reactive astrocytes express the potassium channel Kir4.1 in active multiple sclerosis lesions. *Clin Exp Neuroimmunol*. 2013; **4**: 19–28.
25. van der Valk P, De Groot CJ. Staging of multiple sclerosis (MS) lesions: pathology of the time frame of MS. *Neuropathol Appl Neurobiol*. 2000; **26**: 2–10.
26. Satoh J, Tabunoki H, Ishida T, Saito Y, Arima K. Accumulation of a repulsive axonal guidance molecule RGMa in amyloid plaques: a possible hallmark of regenerative failure in Alzheimer's disease brains. *Neuropathol Appl Neurobiol*. 2013; **39**: 109–20.
27. Hanamsagar R, Torres V, Kielian T. Inflammasome activation and IL-1β/IL-18 processing are influenced by distinct pathways in microglia. *J Neurochem*. 2011; **119**: 736–48.
28. Matute C, Torre I, Pérez-Cerdá F, Pérez-Samartín A, Alberdi E, Etxebarria E, et al. $P2X_7$ receptor blockade prevents ATP excitotoxicity in oligodendrocytes and ameliorates experimental autoimmune encephalomyelitis. *J Neurosci*. 2007; **27**: 9525–33.
29. Yiangou Y, Facer P, Durrenberger P, Chessell IP, Naylor A, Bountra C, et al. COX-2, CB2 and P2X7-immunoreactivities are increased in activated microglial cells/macrophages of multiple sclerosis and amyotrophic lateral sclerosis spinal cord. *BMC Neurol*. 2006; **6**: 12.
30. Gandelman M, Peluffo H, Beckman JS, Cassina P, Barbeito L. Extracellular ATP and the $P2X_7$ receptor in astrocyte-mediated motor neuron death: implications for amyotrophic lateral sclerosis. *J Neuroinflammation*. 2010; **7**: 33.
31. Rajamäki K, Nordström T, Nurmi K, Åkerman KE, Kovanen PT, Öörni K, et al. Extracellular acidosis is a novel danger signal alerting innate immunity via the NLRP3 inflammasome. *J Biol Chem*. 2013; **288**: 13410–9.
32. Adachi T, Takahara K, Taneo J, Uchiyama Y, Inaba K. Particle size of latex beads dictates IL-1β production mechanism. *PLoS ONE*. 2013; **8**: e68499.
33. Lööv C, Hillered L, Ebendal T, Erlandsson A. Engulfing astrocytes protect neurons from contact-induced apoptosis following injury. *PLoS ONE*. 2012; **7**: e33090.
34. Fischer MT, Sharma R, Lim JL, Haider L, Frischer JM, Drexhage J, et al. NADPH oxidase expression in active multiple sclerosis lesions in relation to oxidative tissue damage and mitochondrial injury. *Brain*. 2012; **135**: 886–99.
35. Misawa T, Takahama M, Kozaki T, Lee H, Zou J, Saitoh T, et al. Microtubule-driven spatial arrangement of mitochondria promotes activation of the NLRP3 inflammasome. *Nat Immunol*. 2013; **14**: 454–60.
36. Inoue M, Williams KL, Oliver T, Vandenabeele P, Rajan JV, Miao EA, et al. Interferon-β therapy against EAE is effective only when development of the disease depends on the NLRP3 inflammasome. *Sci Signal*. 2012; **5**: ra38.
37. Inoue M, Williams KL, Gunn MD, Shinohara ML. NLRP3 inflammasome induces chemotactic immune cell migration to the CNS in experimental autoimmune encephalomyelitis. *Proc Natl Acad Sci USA*. 2012; **109**: 10480–5.
38. Wang X, Fu S, Wang Y, Yu P, Hu J, Gu W, et al. Interleukin-1β mediates proliferation and differentiation of multipotent neural precursor cells through the activation of SAPK/JNK pathway. *Mol Cell Neurosci*. 2007; **36**: 343–54.

Supporting Information

Additional Supporting Information may be found in the online version of this article:

Figure S1. The specificity of anti-NLRP3, ASC and caspase-1 (CASP1) antibodies.

Figure S2. The expression of NLRP3 inflammasome components in normal control brains.

Table S1. Human brain tissues examined in the present study.

BRAIN RESEARCH 1499 (2013) 61–68

Available online at www.sciencedirect.com

SciVerse ScienceDirect

www.elsevier.com/locate/brainres

Brain Research

Research Report

Multimodal image analysis of sensorimotor gating in healthy women

Miho Ota[a,*], *Noriko Sato*[b], *Junko Matsuo*[a], *Yukiko Kinoshita*[a], *Yumiko Kawamoto*[a], *Hiroaki Hori*[a], *Toshiya Teraishi*[a], *Daimei Sasayama*[a], *Kotaro Hattori*[a], *Satoko Obu*[a], *Yasuhiro Nakata*[b], *Hiroshi Kunugi*[a]

[a]*Department of Mental Disorder Research, National Institute of Neuroscience, National Center of Neurology and Psychiatry, 4-1-1 Ogawa-Higashi, Kodaira, Tokyo 187–8502, Japan*

[b]*Department of Radiology, National Center of Neurology and Psychiatry, 4-1-1 Ogawa-Higashi, Kodaira, Tokyo 187-8551, Japan*

ARTICLE INFO

Article history:
Accepted 29 December 2012
Available online 16 January 2013

Keywords:
Diffeomorphic anatomical registration using exponentiated lie algebra
Diffusion tensor imaging
Prepulse inhibition
Tract-based spatial statistics

ABSTRACT

Prepulse inhibition (PPI) deficits have been reported in individuals with schizophrenia and other psychiatric disorders with dysfunction of the cortico–striato–pallido–thalamic circuit. The purpose of this study was to investigate the structural neural correlates of PPI by using magnetic resonance imaging (MRI) metrics. The subjects were 53 healthy women (mean age; 40.7±11.3 years). We examined the possible relationships between PPI and diffusion tensor imaging (DTI) metrics to estimate white matter integrity and gray matter volume analyzed using the DARTEL (diffeomorphic anatomical registration through exponentiated lie) algebra method. There were significant correlations between DTI metrics and PPI in the parahippocampal region, the anterior limb of the internal capsule, the ventral tegmental area, the thalamus and anterior thalamic radiations, the left prefrontal region, the callosal commissural fiber, and various white matter regions. There were also positive correlations between PPI and gray matter volume in the bilateral parietal gyri and the left inferior prefrontal gyrus at a trend level. The present study revealed evidence of a relationship between PPI and the integrity of white matter. This result was compatible with the previous suggestion that PPI would be modulated by the cortico-striato-thalamic-pallido-pontine circuit.

Abbreviations: 3-dimensional (3D), blood oxygenation level-dependent (BOLD); cerebrospinal fluid (CSF), diffeomorphic anatomical registration using exponentiated lie algebra (DARTEL); diffusion tensor imaging (DTI), echo time (TE); false discovery rate (FDR), family-wise error (FWE); field of view (FOV), fluid attenuation inversion recovery (FLAIR); fractional anisotropy (FA), functional magnetic resonance imaging (fMRI); mean diffusivity (MD), Mini-International Neuropsychiatric Interview (MINI); positron emission tomography (PET), prepulse inhibition (PPI); repetition time (TR), statistical parametric mapping (SPM); threshold-free cluster enhancement (TFCE), tract-based spatial statistics (TBSS). voxel-based morphometry (VBM).

*Corresponding author. Fax: +81 42 346 2094.
E-mail address: ota@ncnp.go.jp (M. Ota).

0006-8993/$ - see front matter © 2013 Elsevier B.V. All rights reserved.
http://dx.doi.org/10.1016/j.brainres.2012.12.044

1. Introduction

The startle reflex can be attenuated when the startling stimulus is preceded by a weak non-startling prepulse, in a process called prepulse inhibition (PPI). The degree to which such a prepulse inhibits the startle reflex in PPI is used as a measure of sensorimotor gating. Disruptions in information processing and attention have long been thought of as one of the hallmarks of schizophrenia (McGhie and Chapman, 1961), and PPI has been suggested as a neurophysiologic measure of information processing abnormalities in schizophrenia (Cadenhead and Braff, 1999).

There is evidence from animal studies that PPI is modulated by forebrain circuits involving the prefrontal cortex, thalamus, hippocampus, amygdala, nucleus accumbens, striatum, and globus pallidus (Koch and Schnitzler, 1997; Swerdlow and Geyer, 1998; Swerdlow et al., 2001). Deficient PPI is observed in several neuropsychiatric disorders characterised by abnormalities in the cortico-striato-thalamic-pontine circuitry (Braff et al., 2001; Swerdlow et al., 2008). Previous neuroimaging studies using structural brain images revealed the neural correlates of PPI in the prefrontal and orbitofrontal cortex, hippocampus extending to the parahippocampal gyrus, the basal ganglia including parts of putamen, the globus pallidus, and the nucleus accumbens, posterior cingulate, superior temporal gyrus, and thalamus (Kumari et al., 2005, 2008a). Several functional magnetic resonance imaging (fMRI) studies showed that PPI is associated with increased bilateral activation in the striatum extending to the hippocampus, insula, thalamus, and inferior frontal, middle temporal, and inferior parietal lobes (Hazlett et al., 2001, 2008; Kumari et al., 2003, 2008a). A regression analysis demonstrated a linear relationship between PPI and blood oxygenation level-dependent (BOLD) activity in the thalamus, nucleus accumbens, and inferior parietal region (Kumari et al., 2003). Positron emission tomography (PET) study also detected an association between PPI and the prefrontal and inferior parietal cortices' glucose metabolism (Hazlett et al., 1998). Although it is known that PPI disruption resulted from the interruption of the cortico–striato–thalamic–pontine neural circuit, to our knowledge there has been no study verifying the integrity of white matter using diffusion tensor imaging (DTI).

The present study was conducted to investigate the structural basis of PPI deficits using DTI and volumetry analysis. We hypothesized that PPI would be correlated with components in the hippocampus/temporal lobe, basal ganglia, cingulate gyrus, and frontal and parietal regions.

2. Results

Initially, we examined the correlation between the gray matter volume and % PPI using DARTEL (diffeomorphic anatomical registration using exponentiated lie). There was no significant correlation between them; however, there were nominal trends between % PPI with 90 dB prepulse and gray matter volume in the bilateral parietal gyri and left inferior prefrontal regions ($p<0.005$ uncorrected) (Fig. 1(A)), and between % PPI with 86 dB prepulse and gray matter volume in the left parietal and medial frontal regions ($p<0.005$ uncorrected) (Fig. 1(B)).

We then examined correlation between % PPI and DTI. Significant positive correlations were observed between fractional anisotropy (FA) value and % PPI with 90 dB prepulse in the right ventral tegmental area, left anterior limbs of the internal capsule, bilateral thalami, and the left inferior prefrontal region, bilateral medial frontal regions, and bilateral parietal regions ($p<0.001$ uncorrected) (Fig. 2(A) to (F)), however, we could detect correlation between % PPI with 86 dB prepulse and FA values only in the inferior prefrontal region (Fig. 2(G)) ($p<0.001$ uncorrected). In addition, analysis using the skeletonized FA data showed that there were significant positive correlations between FA value and % PPI with 90 dB prepulse in the parahippocampal region, orbitofrontal region, bilateral temporal–inferior parietal regions, internal capsule,

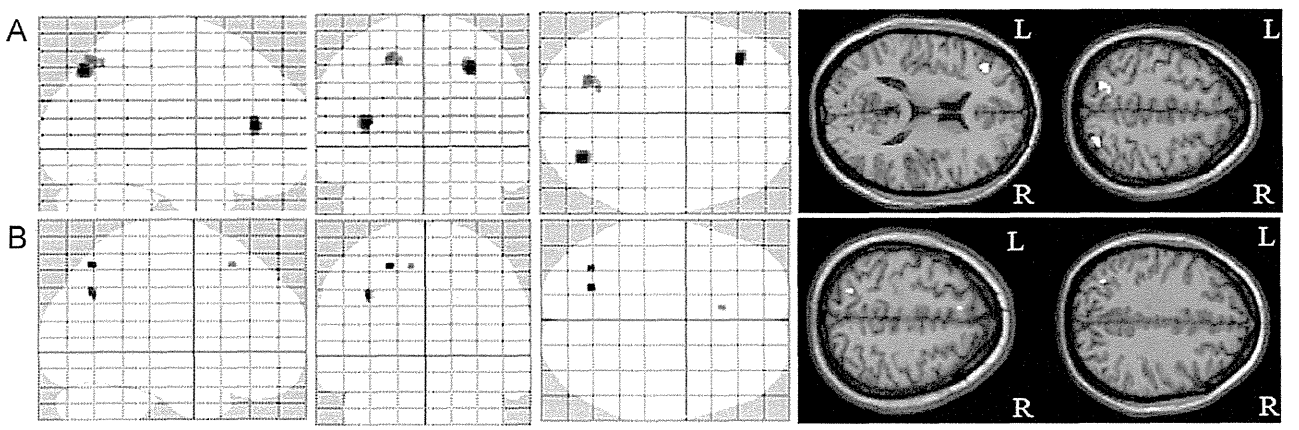

Fig. 1 – Brain areas in which % PPI and gray matter volume showed correlation. There was no significant correlation between % PPI and gray matter volume. However, a nominal trend was found in the bilateral parietal regions and left inferior prefrontal regions (A) ($p<0.005$ uncorrected). Likewise, there was a nominal correlation between % PPI with 86 dB prepulse and gray matter volume in the left parietal and medial frontal regions (B) ($p<0.005$ uncorrected). Age and whole brain volume were controlled. L, left; R, right.

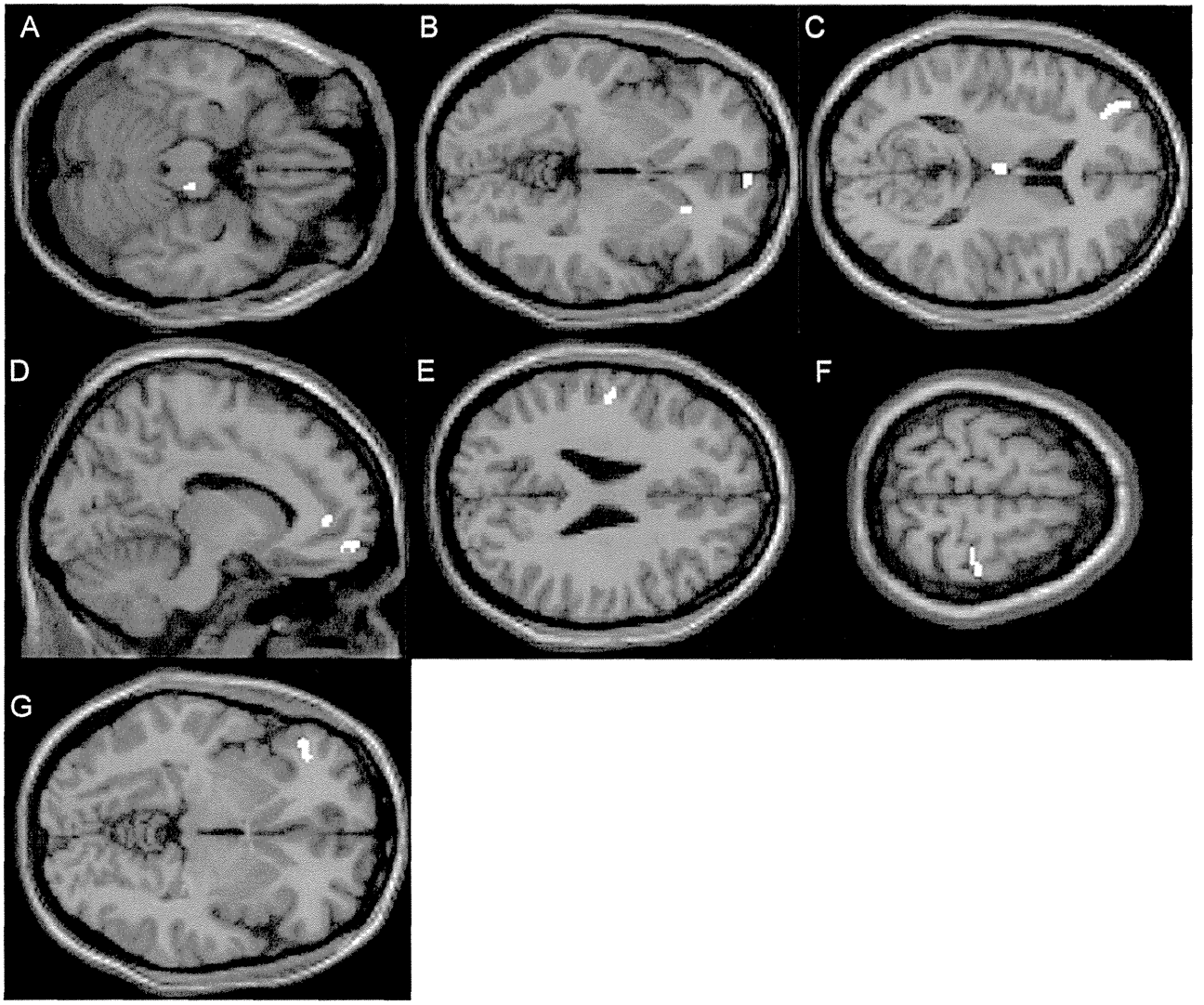

Fig. 2 – Brain areas in which % PPI and FA values correlated. There were positive correlations between % PPI with 90 dB of prepulse and FA values in the right ventral tegmental area (A), left anterior limbs of internal capsule (B), bilateral thalami, and left inferior prefrontal region (C), bilateral medial frontal regions ((B), (D)), and bilateral parietal regions ((E) and (F)) ($p<0.001$ uncorrected). Correlation between % PPI with 86 dB of prepulse and FA values was seen only in the inferior prefrontal region (G) ($p<0.001$ uncorrected). Age was controlled. L, left; R, right.

thalamus, anterior thalamic radiations, posterior cingulate, and callosal commissural fibers ($p<0.05$, family-wise error (FWE) rate is controlled) (Fig. 3(A) to (D)). On the other hand, there were no significant correlation between % PPI with 86 dB prepulse and FA value, and only nominal trends were revealed in similar regions (Fig. 3(E) to (H)) ($p<0.1$; FWE rate is controlled).

There were significantly positive correlations between % PPI and the mean diffusivity (MD) values in many regions throughout the brain (90 dB; Fig. 4(A), 86 dB; Fig. 4(B)). To be more conservative, we corrected for multiple testing by false discovery rate (FDR) and set the critical p-value as <0.01(90 dB), and by FWE and set the critical p-value as <0.05 (86 dB). After this procedure, the correlations of PPI with MD values in the left inferior prefrontal region remained significant (Fig. 4(A) and (B), the right column).

3. Discussion

To our knowledge, this is the first study that used DTI to examine the possible relationships between PPI and brain structure in healthy subjects. Significant correlations were noted between PPI and DTI metrics in the ventral tegmental area, parahippocampus, callosal commissural fiber, thalamus, anterior thalamic radiation, internal capsule, posterior cingulate, and temporal and parietal regions. There were nominal trends between PPI and gray matter volume in the left inferior prefrontal region and bilateral parietal regions. Our results are consistent with previous neuroimaging studies using structural MRI and fMRI and pharmacological studies (Hazlett et al., 2001; Kumari et al., 2005; Swerdlow et al., 2001).

Consistent with the consensus regarding PPI in the rat, a number of psychiatric and neurological disorders characterized

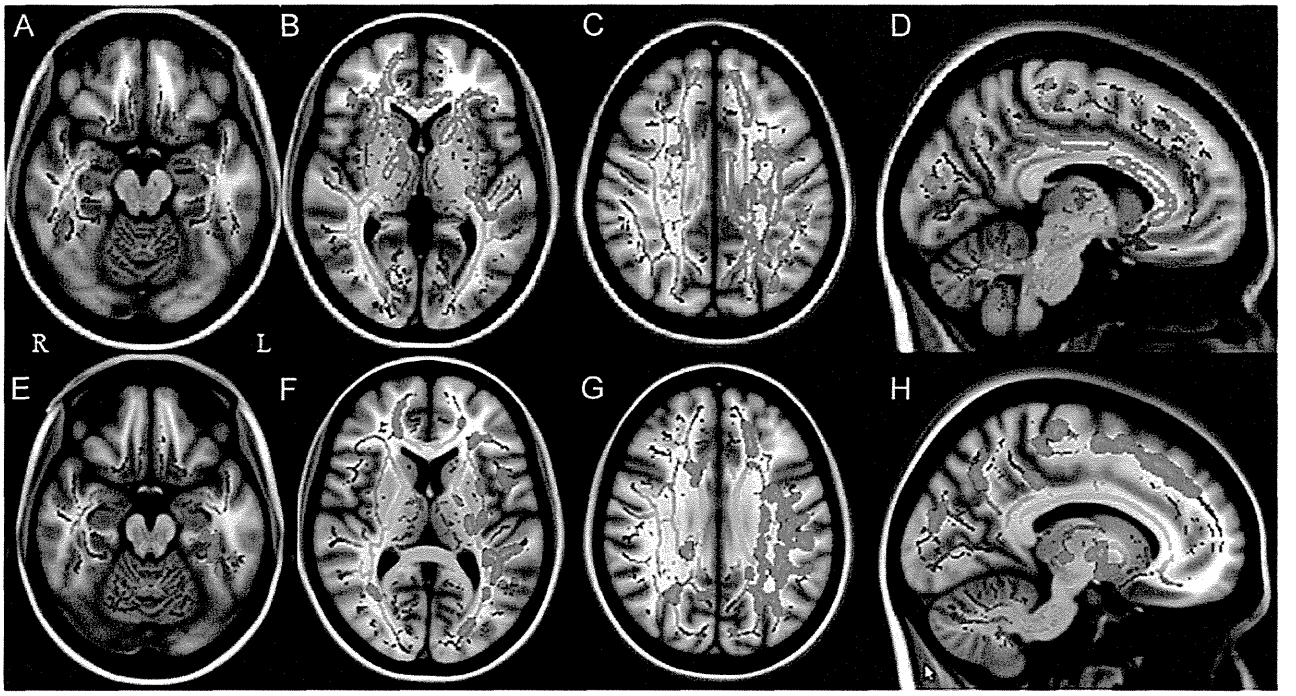

Fig. 3 – Brain areas in which % PPI and FA values correlated using TBSS. There were positive correlations between % PPI with 90 dB of prepulse and FA values in the parahippocampal region (A), orbitofrontal region (A), temporal–parietal regions ((B) and (C)), internal capsules (B), thalamus and anterior thalamic radiations ((B) and (C)), posterior cingulate ((C) and (D)), and anterior dominant callosal commissural fibers ((B) and (D)) revealed by tract-based spatial statistics (TBSS) ($p<0.05$; family-wise error rate is controlled). On the other hand, there were no significant correlations between % PPI with 86 dB of prepulse and FA values, however, a nominal trend was detected in similar regions ((E) to (H)) ($p<0.1$; family-wise error rate is controlled). Age was controlled. The skeleton, shown in green, is thresholded at 0.2 and overlaid onto the MNI152 space. L, left; R, right. (For interpretation of the references to colour in this figure legend, the reader is referred to the web version of this article.)

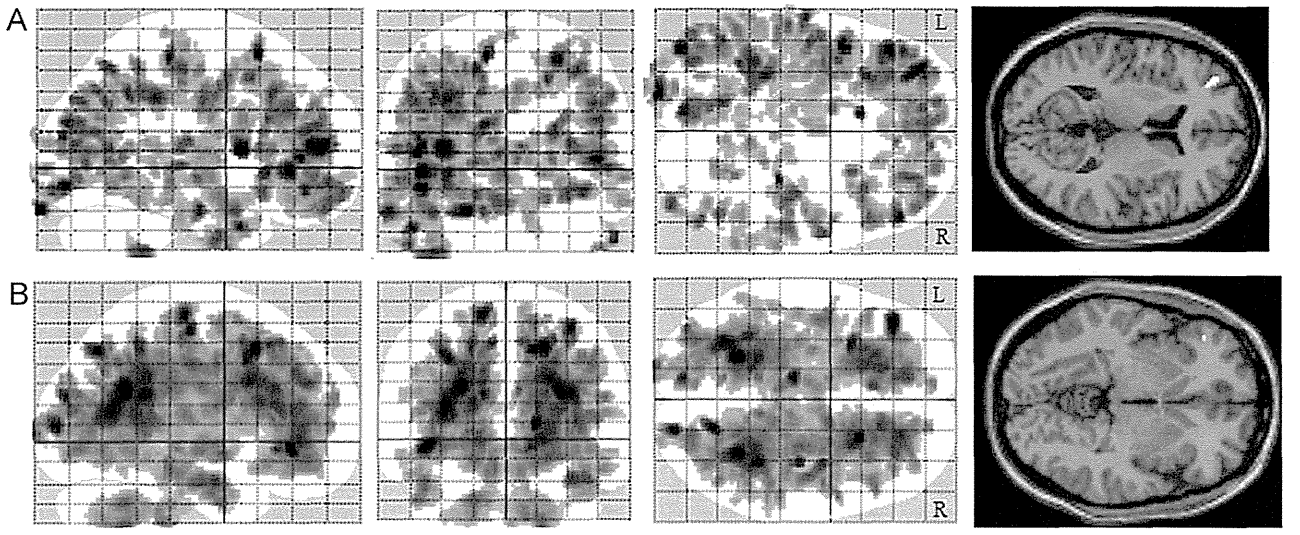

Fig. 4 – Brain areas in which % PPI and MD values correlated. There were negative correlations between % PPI with 90 (A) and 86 dB (B) of prepulse and MD values in several areas throughout the brain ($p<0.001$ uncorrected). The right column showed that the correlations remained when we re-analyzed the correlation between PPI and MD values in the left inferior prefrontal region (90 dB; $p<0.01$ [false discovery rate], 86 dB; $p<0.05$ [family-wise error rate]). L, left; R, right.

by abnormalities at some level in the cortico–striato–thalamic–pontine circuitry (Braff et al., 2001; Swerdlow et al., 2008) and in the cortico–striato–pallido–thalamic brain substrate (Perry et al., 2004; Swerdlow et al., 2008) showed the PPI deficient. Previous neuroimaging studies revealed the correlation between PPI and regional brain using structural brain images (Kumari et al., 2005,

2008b), and fMRI (Hazlett et al., 2001, 2008; Kumari et al., 2003, 2007, 2008a). Here we found significant correlations between PPI and DTI metrics in the parahippocampus, the internal capsule, the circumference of anterior thalamic radiation and the parietal region. In light of these observations, PPI may be regulated through an amygdala – basal ganglia – prefrontal and parietal circuit. There is evidence from animal studies that PPI is mediated by brain stem circuits involving the inferior colliculus, superior colliculus, pedunculopontine tegmental nucleus, laterodorsal tegmental nucleus, substantia nigra pars reticulata, and caudal pontine reticular nucleus (Fendt et al., 2001). In the present study, we detected a correlation between FA in the ventral tegmental area and % PPI, a finding that is compatible with this previous evidence.

As described above, previous studies showed that PPI is influenced by many regions throughout the brain, and PPI is thought to be affected by the transmission of information. We therefore hypothesized that to evaluate the relation between PPI and the brain, the use of DTI – which shows the condition of the neural fibers – would be effective. Our DTI results suggested that a large area of the brain is involved in deficits in PPI, compared to the foregoing studies focusing on the gray matter. This may be due to the ability of DTI to delineate neural pathways. Furthermore, we detected more correlations between % PPI and brain metrics when prepulse was 90 dB than when it was 86 dB. Previous studies showed that % PPI at the prepulse intensity of 90 dB was higher compared with that at 86 dB, and that the difference in % PPI between patients with schizophrenia and healthy controls became most significant when prepulse was 90 dB (Kunugi et al., 2007; Takahashi et al., 2008; Moriwaki et al., 2009). These points may suggest that % PPI with 90 dB of prepulse is the best condition to reflect his/her own information processing and attention.

Regarding the volumetric analysis, we could not detect any significant relationship between the PPI and gray matter volume, although the data showed a nominal trend of a relationship in the inferior frontal gyrus and bilateral parietal regions. As to the association between the inferior prefrontal region and PPI, we detected this relationship by all metrics used in this study. This connection was previously detected in an MRI volumetric study (Kumari et al., 2005). However, 10 men and 14 women took part in that study. Previous studies showed a gender difference in PPI (Kumari. et al., 2004), but we evaluated only female subjects. We failed to detect any significant correlation between PPI and gray matter volume. The inconsistent results between previous studies and ours may be attributable, at least in part, to the fact that we examined only females who showed a narrow range of PPI. In conjunction with this, our study included only healthy women whose % PPI was changeable along with the menstrual cycle status (Swerdlow et al., 1997). Further studies work with information on menstrual cycle and studies on male subjects are necessary to address this issue.

In conclusion, the present study examined structural neural correlates of PPI and revealed evidence of a relationship between PPI and the integrity of white matter in healthy women. These observations confirm the involvement of these regions in human PPI as suggested by previous relevant data. Further research should extend the present methods in studies of clinical populations.

4. Experimental procedures

4.1. *Sample*

The subjects were 63 healthy females who were recruited from the community through local magazine advertisements and our website announcement. The participants were interviewed for enrollment using the Japanese version of the Mini-International Neuropsychiatric Interview (MINI) (Otsubo et al., 2005; Sheehan et al., 1998) by research psychiatrists, and only those who demonstrated no history of psychiatric illness or contact with psychiatric services were enrolled in the study. Participants were excluded if they had a prior medical history of central nervous system disease or severe head injury. In addition, 10 non-responders to the startle stimulus (see the "*Prepulse inhibition measure*" below) were also excluded from the analysis. As a consequence, 53 healthy females (mean age; 40.7±11.3 years, education; 14.8±2.7 years) took part in the study.

Written informed consent was obtained for participation in the study from all subjects, and the study was approved by the Ethics Committee of the National Center of Neurology and Psychiatry, Tokyo, Japan.

4.2. *Prepulse inhibition measure*

Our equipment, setup, and standard PPI testing procedures have been described in detail (Kunugi et al., 2007). The startle reflex to acoustic stimuli was measured using the Startle Reflex Test Unit for Humans (O'Hara Medical, Tokyo). Subjects refrained from smoking for at least 20 min prior to the test. Broadband white noise (50 to 24,000 Hz) at 70 dB was presented as the background noise and was continuous throughout the session. Acoustic startle stimuli of the broadband white noise were presented through headphones.

During the initial 3 min of each session, the background noise alone was given for acclimation. In total, 35 startle-response trials were recorded in a session. These trials consisted of three blocks. In the first block, the subject's startle response to a pulse (sound pressure: 115 dB; duration: 40 ms) alone was recorded five times. In the second block, the subject's startle response to the same pulse with or without a prepulse (sound pressure: 86 or 90 dB; duration: 20 ms; lead interval [onset to onset]: 60 or 120 ms) was measured five times for each condition. The differential conditions of trials were presented in a pseudo-random order; however, the order was the same for all of the subjects. In the third and final block, the startle response to the pulse alone was again measured five times. The intertrial intervals (15 s on average, range 10 to 20 s) were randomly changed. The entire session lasted approximately 15 min. The mean % PPI of startle magnitude was calculated using the following formula, because in a previous study this condition showed the best sensitivity to differentiate between schizophrenic patients and healthy subjects (Kunugi et al., 2007):

% PPI=100 × (magnitude on pulse-alone trials−magnitude on prepulse trials {sound pressure: 86 dB and 90 dB; lead

interval: 120 ms, right eye])/magnitude on pulse-alone trials in the 2nd block.

The mean % PPI of the 53 subjects were 45.9±54.7 under the terms of 86 dB, and 58.8±39.8 of 90 dB. We defined *a priori* the "non-responders" to the startle stimuli as those subjects for whom the average value of the startle magnitude in the pulse-alone trials was <0.05 (digital unit), and the non-responders were excluded from the analysis.

4.3. MRI data acquisition

4.3.1. *Data acquisition*

MR imaging was performed on a Magnetom Symphony 1.5-T system (Siemens, Erlangen, Germany). High spatial resolution, 3-dimensional (3D) T1-weighted images of the brain were obtained for the morphometric study. The 3D T1-weighted images were scanned in the sagittal plane (echo time (TE)/repetition time (TR): 2.64/1580 ms; flip angle: 15°; effective slice thickness: 1.23 mm; slab thickness: 177 mm; matrix: 208 × 256; field of view (FOV): 256 × 315 mm^2; acquisition: (1), yielding 144 contiguous slices through the head.

DTI was performed in the axial plane (TE/TR: 106/11,200 ms; FOV: 240 × 240 mm^2; matrix: 96 × 96; 75 continuous transverse slices; slice thickness 2.5 mm with no interslice gap; acquisitions: (2). Diffusion was measured along 12 non-collinear directions with the use of a diffusion-weighted factor, *b*, in each direction for 1000 s/mm^2, and one image was acquired without use of a diffusion gradient. The DTI examination took approx. 6 min. In addition to DTI and 3D T1-weighted images, conventional axial T2-weighted images (TE/TR: 95/3500 ms; flip angle: 150°; slice thickness: 5 mm; intersection gap: 1.75 mm; matrix: 448 × 512; FOV: 210 × 240 mm^2; acquisitions: (1), and fluid attenuation inversion recovery (FLAIR) images in the axial plane (TE/TR: 101/8800 ms; flip angle: 150°; slice thickness: 3 mm; intersection gap: 1.75 mm; matrix: 448 × 512; FOV: 210 × 240 mm^2; acquisition: (1) were acquired to exclude cerebrovascular disease. On conventional MRI, no abnormal findings were detected in the brain in any subject.

4.3.2. *Diffeomorphic anatomical registration using exponentiated lie analysis*

The raw 3D T1-weighted volume data were transferred to a workstation. A preprocessing step of voxel-based morphometry (VBM) in Statistical Parametric Mapping (SPM) was improved with the DARTEL registration method (Ashburner, 2007). This technique, being more deformable, notably improves the realignment of small inner structures (Yassa and Stark, 2009). Calculations and image matrix manipulations were performed using SPM8 running on MATLAB R2007a software (MathWorks, Natick, MA). MR imaging data were analyzed using DARTEL as a toolbox for SPM8 to create a set of group-specific templates. The brain images were segmented, normalized, and modulated by using these templates. The output images were still in the average brain space. Additional warping from the Montreal Neurologic Institute space was given to the brain images. Then, gray matter probability values were smoothed by using an 8-mm full-width at half-maximum Gaussian kernel.

4.3.3. *DTI procedure*

The DTI data sets were analyzed using DtiStudio (Jiang et al., 2006). The diffusion tensor parameters were calculated on a pixel-by-pixel basis, and FA and MD map and $b=0$ image were calculated according to Wakana et al. (2004).

4.3.4. *SPM analysis*

To estimate the relationships between brain morphology and % PPI, FA and MD images were analyzed using an optimized VBM technique. The data were analyzed using SPM5 software running on MATLAB 7.0. The images were processed using an optimized VBM script. The details of this process are described elsewhere (Good et al., 2001). First, each individual 3D-T1 image was coregistered and resliced to its own $b=0$ image. Next, the coregistered 3D-T1 image was normalized to the "avg152T1" image regarded as the anatomically standard image in SPM5. Finally, the transformation matrix was applied to FA and MD maps. Further, to avoid the effect of diffusivity of cerebrospinal fluid (CSF), MD images were masked with the CSF image derived from the segmented individual 3D-T1 image. Each map was then spatially smoothed with a 6-mm full-width at half-maximum Gaussian kernel in order to decrease spatial noise and compensate for the inexactitude of normalization following the "rule of thumb" developed for fMRI and PET studies (Snook et al., 2007).

4.3.5. *Tract-based spatial statistics (TBSS) analysis*

The processing technique known as "tract-based spatial statistics (TBSS) analysis" projects DTI data onto a common pseudo-anatomical skeleton instead of trying to match each and every voxel in different subjects, and therefore does not need smoothing (Smith et al., 2006). TBSS is available as part of the FSL 4.1 software package (Smith et al., 2004). The TBSS script runs a nonlinear registration, aligning all FA images to the FMRIB58_FA template, which is supplied with FSL. The script then takes the target and affine-aligns it into a 1 × 1 × 1 mm MNI152 space. Once this is done, each subject's FA image has the nonlinear transform to the target and then the affine transform to MNI152 space is applied, resulting in a transformation of the original FA image into MNI152 space. Next, TBSS creates the mean of all aligned FA images and applies thinning of the local tract structure to create a skeletonized mean FA image. In order to exclude areas of low FA and/or high intersubject variability from a statistical analysis, TBSS thresholds a mean FA skeleton with a certain FA value, typically 0.2. The resulting binary skeleton mask is a pseudo-anatomical representation of the main fiber tracks, and defines the set of voxels used in all subsequent processing. Finally, TBSS projects each subject's aligned FA image onto the skeleton. This results in skeletonized FA data. It is this file that is used for the voxelwise statistics.

4.3.6. *Statistical analysis*

Statistical analyses were performed using SPM5 software (Welcome Department of Imaging Neuroscience, London, UK). Correlations between regional gray matter volume and % PPI with 86 and 90 dB of prepulse were assessed using the subjects' age, length of education, and whole brain volume as nuisance variables, and FA and MD value maps and % PPI

were assessed using age and education year as nuisance variables. Only correlations that met these criteria were deemed significant. In this case, a seed level of $p<0.001$ (uncorrected) and a cluster level of $p<0.05$ (uncorrected) were selected.

Skeletonized FA data were analyzed for revealing correlations with % PPI, controlling for age, using the FSL "Threshold-Free Cluster Enhancement (TFCE)" option in "randomise" with 5000 permutations, the script of which uses a permutation-based statistical inference that does not rely on a Gaussian distribution of voxels, and is run without having to define an initial cluster-forming threshold or carry out a large amount of data smoothing (Nichols and Holmes, 2002; Smith and Nichols, 2009). The significance level was set at the p-value of less than 0.05 with FWE rate correction for multiple comparisons.

Acknowledgments

This study was supported by Health and Labor Sciences Research Grants (Comprehensive Research on Disability, Health, and Welfare), Intramural Research Grant (24-11) for Neurological and Psychiatric Disorders of NCNP (M.O. and H.K.), "Understanding of molecular and environmental bases for brain health" carried out under the Strategic Research Program for Brain Sciences by the Ministry of Education, Culture, Sports, Science and Technology of Japan, and a grant from Core Research of Evolutional Science & Technology (CREST), Japan Science and Technology Agency (JST) (H.K.)

REFERENCES

Ashburner, J., 2007. A fast diffeomorphic image registration algorithm. NeuroImage 38, 95–113.

Braff, D.L., Geyer, M.A., Swerdlow, N.R., 2001. Human studies of prepulse inhibition of startle: normal subjects, patient groups, and pharmacological studies. Psychopharmacology (Berl) 156, 234–258.

Cadenhead, K.S., Braff, D.L., 1999. Schizophrenia spectrum disorders. In: Dawson, M.E., Schell, A.M., Bohmelt, A.H. (Eds.), Startle Modification: Implications for Neuroscience. Cognitive Science, and Clinical Science. Cambridge University Press, Cambridge, pp. 231–244.

Fendt, M., Liang, L., Yeomans, J.S., 2001. Brain stem circuits mediating prepulse inhibition of the startle reflex. Psychopharmacology 156, 216–224.

Good, C.D., Johnsrude, I., Ashburner, J., Henson, R.N.A., Friston, K.J., Frackowiak, R.S.J., 2001. Cerebral asymmetry and the effect of sex and handedness on brain structure: a voxel-based morphometric analysis of 465 normal adult human brains. NeuroImage 14, 685–700.

Hazlett, E.A., Buchsbaum, M.S., Haznedar, M.M., Singer, M.B., Germans, M.K., Schnur, D.B., Jimenez, E.A., Buchsbaum, B.R., Troyer, B.T., 1998. Prefrontal cortex glucose metabolism and startle eyeblink modification abnormalities in unmedicated schizophrenia patients. Psychophysiology 35, 186–198.

Hazlett, E.A., Buchsbaum, M.S., Tang, C.Y., Fleischman, M.B., Wei, T.C., Byne, W., Haznedar, M.M., 2001. Thalamic activation during an attention-to-prepulse startle modification paradigm: a functional MRI study. Biol. Psychiatry 50, 281–291.

Hazlett, E.A., Buchsbaum, M.S., Zhang, J., Newmark, R.E., Glanton, C.F., Zelmanova, Y., Haznedar, M.M., Chu, K.W., Nenadic, I., Kemether, L.J., Tang, C.Y., New, A.S., Siever, L.J., 2008. Frontal–striatal–thalamic mediodorsal nucleus dysfunction in schizophrenia-spectrum patients during sensorimotor gating. NeuroImage 42, 1164–1177.

Jiang, H., van Zijil, P.C., Kim, J., Pearlson, G.D., Mori, S., 2006. DtiStudio: resource program for diffusion tensor computation and fiber bundle tracking. Comput. Methods Programs Biomed. 81, 106–116.

Koch, M, Schnitzler, H, 1997. The acoustic startle response in rats: circuits mediating evocation, inhibition and potentiation. Behav. Brain Res. 89, 35–49.

Kumari, V., Aasen, I., Sharma, T., 2004. Sex differences in prepulse inhibition deficits in chronic schizophrenia. Schizophr. Res. 69, 219–235.

Kumari, V., Antonova, E., Geyer, M.A., 2008a. Prepulse inhibition and "psychosis-proneness" in healthy individuals: an fMRI study. Eur. Psychiatry 23, 274–280.

Kumari, V., Antonova, E., Geyer, M.A., Ffytche, D., Williams, S.C., Sharma, T., 2007. A fMRI investigation of startle gating deficits in schizophrenia patients treated with typical or atypical antipsychotics. Int. J. Neuropsychopharmacol. 10, 463–477.

Kumari, V., Antonova, E., Zachariah, E., Galea, A., Aasen, I., Ettinger, U., Mitterschiffthaler, M.T., Sharma, T., 2005. Structural brain correlates of prepulse inhibition of the acoustic startle response in healthy humans. NeuroImage 26, 1052–1058.

Kumari, V., Fannon, D., Geyer, M.A., Premkumar, P., Antonova, E., Simmons, A., Kuipers, E., 2008b. Cortical grey matter volume and sensorimotor gating in schizophrenia. Cortex 44, 1206–1214.

Kumari, V., Gray, J.A., Geyer, M.A., Ffytche, D., Mitterschiffthaler, M.T., Vythelingum, G.N., Williams, S.C.R., Simmons, A., Sharma, T., 2003. Neural correlates of prepulse inhibition in normal and schizophrenic subjects: a functional MRI Study. Psychiatry Res.: NeuroImage 122, 99–113.

Kunugi, H., Tanaka, M., Hori, H., Hashimoto, R., Saitoh, O., Hironaka, N., 2007. Prepulse inhibition of acoustic startle in Japanese patients with chronic schizophrenia. Neurosci. Res. 59, 23–28.

McGhie, A, Chapman, J., 1961. Disorders of attention and perception in early schizophrenia. Br. J. Med. Psychol. 34, 103–116.

Moriwaki, M., Kishi, T., Takahashi, H., Hashimoto, R., Kawashima, K., Okochi, T., Kitajima, T., Furukawa, O., Fujita, K., Takeda, M., Iwata, N., 2009. Prepulse inhibition of the startle response with chronic schizophrenia: a replication study. Neurosci. Res. 65, 259–262.

Nichols, T.E., Holmes, A.P., 2002. Nonparametric permutation tests for functional neuroimaging: a primer with examples. Hum. Brain. Mapp. 15, 1–25.

Otsubo, T., Tanaka, K., Koda, R., Shinoda, J., Sano, N., Tanaka, S., Aoyama, H., Mimura, M., Kamijima, K., 2005. Reliability and validity of Japanese version of the Mini-International Neuropsychiatric Interview. Psychiatry Clin. Neurosci. 59, 517–526.

Perry, W., Minassian, A., Feifel, D., 2004. Prepulse inhibition in patients with non-psychotic major depressive disorder. J. Affect. Disord. 81, 179–184.

Sheehan, D.V., Lecrubier, Y., Sheehan, K.H., Amorim, P., Janavs, J., Weiller, E., Hergueta, T., Baker, R., Dunbar, G.C., 1998. The Mini-International Neuropsychiatric Interview (M.I.N.I.): the development and validation of a structured diagnostic psychiatric interview for DSM-IV and ICD-10. J. Clin. Psychiatry 59, 22–57.

Smith, S.M., Jenkinson, M., Johansen-Berg, H., Rueckert, D., Nichols, T.E., Mackay, C.E., Watkins, K.E., Ciccarelli, O., Cader, M.Z., Matthews, P.M., Behrens, T.E., 2006. Tract-based

spatial statistics: voxelwise analysis of multi-subject diffusion data. NeuroImage 31, 1487–1505.

Smith, S.M., Jenkinson, M., Woolrich, M.W., Beckmann, C.F., Behrens, T.E., Johansen-Berg, H., Bannister, P.R., De Luca, M., Drobnjak, I., Flitney, D.E., Niazy, R.K., Saunders, J., Vickers, J., Zhang, Y., De Stefano, N., Brady, J.M., Matthews, P.M., 2004. Advances in functional and structural MR image analysis and implementation as FSL. NeuroImage 23 (1), S208–219.

Smith, S.M., Nichols, T.E., 2009. Threshold-free cluster enhancement: addressing problems of smoothing, threshold dependence and localisation in cluster inference. NeuroImage 44, 83–98.

Snook, L., Plewes, C., Beaulieu, C., 2007. Voxel based versus region of interest analysis in diffusion tensor imaging of neurodevelopment. NeuroImage 34, 243–252.

Swerdlow, N.R., Geyer, M.A., 1998. Using an animal model of deficient sensorimotor gating to study the pathophysiology and new treatments of schizophrenia. Schizophrenia Bull. 24, 285–301.

Swerdlow, N.R., Geyer, M.A., Braff, D.L., 2001. Neural circuit regulation of prepulse inhibition of startle in the rat: current knowledge and future challenges. Psychopharmacology 156, 194–215.

Swerdlow, N.R., Hartman, P.L., Auerbach, P.P., 1997. Changes in sensorimotor inhibition across the menstrual cycle: implications for neuropsychiatric disorders. Biol. Psychiatry 41, 452–460.

Swerdlow, N.R., Weber, M., Qu, Y., Light, G.A., Braff, D.L., 2008. Realistic expectations of prepulse inhibition in translational models for schizophrenia research. Psychopharmacology (Berl) 199, 331–388.

Takahashi, H., Iwase, M., Ishii, R., Ohi, K., Fukumoto, M., Azechi, M., Ikezawa, K., Kurimoto, R., Canuet, L., Nakahachi, T., Iike, N., Tagami, S., Morihara, T., Okochi, M., Tanaka, T., Kazui, H, Yoshida, T, Tanimukai, H, Yasuda, Y, Kudo, T, Hashimoto, R, Takeda, M., 2008. Impaired prepulse inhibition and habituation of acoustic startle response in Japanese patients with schizophrenia. Neurosci. Res. 62, 187–194.

Wakana, S., Jiang, H., Nagae-Poetscher, L.M., van Zijl, P.C., Mori, S., 2004. Fiber tract-based atlas of human white matter anatomy. Radiology 230, 77–87.

Yassa, M.A., Stark, C.E., 2009. A quantitative evaluation of cross-participant registration techniques for MRI studies of the medial temporal lobe. NeuroImage 44, 319–327.

Original Paper

Neuropsychobiology

Neuropsychobiology 2013;68:205–211
DOI: 10.1159/000355298

Received: October 29, 2012
Accepted after revision: August 26, 2013
Published online: November 1, 2013

Hypothalamic-Pituitary-Adrenal Axis Hyperactivity and Brain Differences in Healthy Women

Miho Ota[a] Hiroaki Hori[a] Noriko Sato[b] Daimei Sasayama[a] Kotaro Hattori[a] Toshiya Teraishi[a] Satoko Obu[a] Yasuhiro Nakata[b] Hiroshi Kunugi[a]

[a]Department of Mental Disorder Research, National Institute of Neuroscience, National Center of Neurology and Psychiatry, and [b]Department of Radiology, National Center Hospital, National Center of Neurology and Psychiatry, Kodaira, Japan

Key Words

Dexamethasone · Corticotropin-releasing hormone test · Diffeomorphic anatomical registration using exponentiated Lie algebra · Diffusion tensor imaging · Hypothalamic-pituitary-adrenal system · Magnetic resonance imaging

Abstract

Background: Previous studies have suggested that dysregulation of the hypothalamic-pituitary-adrenal (HPA) axis leads to brain changes. However, few studies have examined the whole brain configuration for an association with HPA axis activity. We examined the relationship between HPA axis activity and the whole brain configuration. ***Methods:*** The subjects in this study were 34 healthy female volunteers. HPA axis activity was assessed by the dexamethasone/corticotropin-releasing hormone test. Structural volumes of the brain and diffusion tensor images were obtained, and correlations were evaluated voxel-wise. ***Results:*** There was a significantly negative correlation between fractional anisotropy value and cortisol levels at 16:00 h (CL-2) in the anterior cingulum, left parahippocampus and right occipital region. There were significantly positive correlations between mean diffusivity value and CL-2 in the left hippocampus and bilateral parahippocampal regions. ***Conclusions:*** Our data suggest that reduced feedback of the HPA axis is associated with reduced neural connectivity throughout the brain, and such an association may be strong in the anterior cingulate, the hippocampus and the parahippocampal regions.

Introduction

The hypothalamic-pituitary-adrenal (HPA) axis plays a central role in stress response and is highly sensitive to everyday challenges in animals and humans [1]. Acute stress activates the HPA axis and triggers the release of cortisol, which is regulated by the negative feedback system in pituitary and hypothalamic regions to inhibit further release [2]. The limbic system, particularly the hippocampus, has also been implicated in the regulation of the HPA axis [2]. Preclinical and clinical studies suggested that increased cortisol levels potentiate adverse effects of neuronal insults, including excess N-methyl-D-aspartate [3], reactive oxygen species [4] and disruption of neuronal calcium homeostasis [5].

Several studies have examined the relationship of regional brain volumes measured by magnetic resonance

M.O. and H.H. contributed equally to this study.

KARGER

E-Mail karger@karger.com
www.karger.com/nps

0302–282X/13/0684–0205$38.00/0

Miho Ota, MD, PhD
Department of Mental Disorder Research, National Institute of Neuroscience
National Center of Neurology and Psychiatry, 4-1-1 Ogawa-Higashi
Kodaira, Tokyo 187-8502 (Japan)
E-Mail ota@ncnp.go.jp

imaging (MRI) with cortisol levels or an impaired negative feedback system of the HPA axis assessed by the dexamethasone (DEX) suppression test and its refined variant, the DEX suppression/corticotropin-releasing hormone (DEX/CRH) test developed by Holsboer et al. [6]. Lupien et al. [7] examined the plasma cortisol level in healthy elderly people in relation to their cognition and neuroimaging variables and found that individuals with increased cortisol levels showed hippocampal atrophy and cognitive decline. In accordance with this, Wolf et al. [8] found a negative correlation between hippocampal volume and 24-hour urinary free cortisol level in healthy men. In contrast, MacLullich et al. [9] reported that hippocampal volume was not significantly associated with cortisol level or impaired HPA axis regulation revealed by the DEX suppression test in healthy men, although the same research group subsequently reported that impaired HPA axis regulation was associated with smaller volume of the left anterior cingulate cortex [10]. Another research group reported that a significant correlation was observed between HPA axis hyperactivity assessed by the DEX/CRH test and frontal lobe atrophy in humans [11]. Indeed, the prefrontal cortex was shown to be a target for glucocorticoids in rats; [^{3}H]DEX binds to receptors in the frontal cortex [12]. Diffusion tensor imaging (DTI) is amongst the most popular imaging techniques for the measurement of the translational displacement of water molecules. The motion or diffusion of water molecules was found to be much faster along the white matter fibers than perpendicular to them. The difference between these two motions (termed 'diffusion anisotropy') is the basis of DTI. DTI provides measures of diffusivity (a measure of mean diffusivity, MD, a quantitative measure of the mean motion of water) and of fractional anisotropy (FA), a measure of the directionality of diffusion [13, 14]. In general, MD is thought to increase with loss of neurons, axons and dendrites, while FA is reduced by a change in tissue cytoarchitecture, likely due to demyelination of axonal structures. Two studies revealed that HPA axis tonus is associated with the hippocampus and the major limbic fiber bundles by using the DTI technique [15, 16]. These previous studies evaluated specific brain regions, i.e. manually placed regions of interest, and to our knowledge there have been few studies that examined the possible association of cortisol level or impaired feedback system of the HPA axis with the whole brain configuration. Furthermore, no study has examined the possible relationship between altered HPA axis and morphology of the whole brain assessed by the DTI technique.

In this study, we tried to elucidate which brain regions are affected by the impaired negative feedback system in the HPA axis in healthy women. HPA axis function was assessed by using the DEX/CRH test. The brain structures were measured by MRI and DTI, and the correlation between HPA axis activity and brain structures was examined voxel-wise.

Methods

Subjects

The subjects were 34 healthy female volunteers (mean age: 48.9 ± 10.7 years; range: 27–65 years), who underwent MRI scanning and the DEX/CRH test; they were recruited from the community via local magazine advertisements and our website announcement. Participants were interviewed for enrollment using the Japanese version of the Mini-International Neuropsychiatric Interview [17, 18] and an additional unstructured interview with the research psychiatrists, and only those who demonstrated no history of psychiatric illness or contact with psychiatric services were enrolled. Participants were excluded if they had a prior medical history of central nervous system disease, severe head injury or other conditions which may affect brain morphology.

Written informed consent was obtained for participation in the study from all subjects, and the study protocol was approved by the ethics committee of the National Center of Neurology and Psychiatry, Japan.

MRI Data Acquisition and Processing

MRI was performed on a Magnetom Symphony 1.5-tesla (Siemens, Erlangen, Germany). High-spatial-resolution, 3-dimensional (3D) T1-weighted images of the brain were obtained for the morphometric study. The 3D T1-weighted images were scanned in the sagittal plane (echo/repetition time, TE/TR: 2.64/1,580 ms; flip angle: 15°; effective slice thickness: 1.23 mm; slab thickness: 177 mm; matrix: 208 × 256; field of view, FOV: 256 × 315 mm^2; acquisitions: 1), yielding 144 contiguous slices through the head. The raw 3D T1-weighted volume data were transferred to a workstation, and structural images were normalized by DARTEL (Diffeomorphic Anatomical Registration through Exponentiated Lie Algebra) analysis [19]. This technique, being more deformable, notably improves the realignment of small inner structures [20]. Calculations and image matrix manipulations were performed by using Statistical Parametric Mapping 8 (SPM8) software (Wellcome Department of Imaging Neuroscience, London, UK) running on Matlab R2007a (Math Works, Natick, Mass., USA). MRI data were analyzed by using DARTEL implemented as a toolbox for SPM8 to create a set of group-specific templates. The brain images were segmented, normalized and modulated by using these templates. The output images were still in the average brain space. Additional warping from the Montreal Neurologic Institute space was given to the brain images. Then, gray matter probability values were smoothed by using a 10-mm full-width at half-maximum Gaussian kernel.

DTI was performed in the axial plane (TE/TR: 106/11,200 ms; matrix: 96 × 96; FOV: 240 × 240 mm^2; 75 continuous transverse slices; slice thickness: 2.5 mm, with no interslice gap) followed by

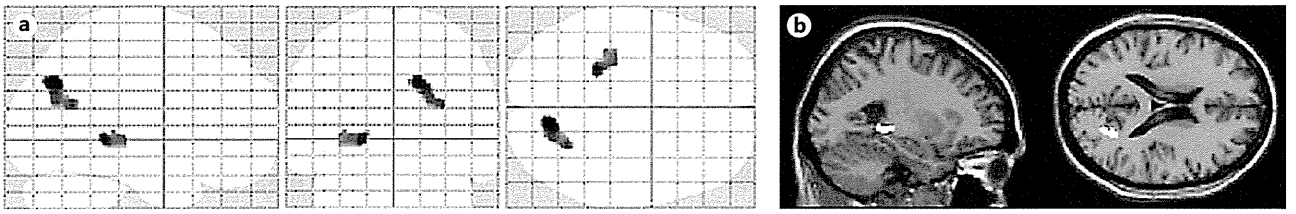

Fig. 1. There were nominal trends between cortisol level at 16:00 h in the DEX/CRH test (**a**) and gray matter volume in the parahippocampal region and right precuneus (**b**). $p < 0.01$, uncorrected. Cluster level; $k > 200$.

MRI. To enhance the signal-to-noise ratio, acquisition was repeated 2 times. Diffusion was measured along 12 noncollinear directions using a diffusion-weighted factor b in each direction for 1,000 s/mm^2, and one image was acquired without using any diffusion gradient. The DTI examination took approximately 6 min. All diffusion-weighted images were visually inspected for apparent artifacts due to subject motion and instrument malfunction. The DTI data were then corrected for eddy current distortion, and the FA and MD maps were calculated on a voxel-by-voxel basis, using the Functional Magnetic Resonance Imaging of the Brain (FMRIB) diffusion toolbox (FDT version 2.0), stored in the FSL (FMRIB Software Library) 4.1 software package [21]. To estimate the relationships between brain morphology and plasma cortisol level after the DEX/CRH test, FA and MD images were normalized to the 'FMRIB58_FA_1mm.nii' image regarded as the anatomical standard image in FSL 4.1. Data were analyzed using SPM8. Each map was then spatially smoothed with a 6-mm full-width at half-maximum Gaussian kernel in order to decrease spatial noise and compensate for the inexactitude of normalization [22]. In addition to DTI and 3D T1-weighted images, conventional axial T2-weighted images (TE/TR: 95/3,500 ms; flip angle: 150°; slice thickness: 5 mm; intersection gap: 1.75 mm; matrix: 448 × 512; FOV: 210 × 240 mm^2; acquisitions: 1) and fluid attenuated inversion recovery images in the axial plane (TE/TR: 101/8,800 ms; flip angle: 150°; slice thickness: 3 mm; intersection gap: 1.75 mm; matrix: 448 × 512; FOV: 210 × 240 mm^2; acquisition: 1) were acquired to exclude cerebrovascular disease. On conventional MRI, no abnormal findings were detected in the brain, sella or parasellar areas in any subject.

We regarded gray matter volume plus white matter volume as the whole brain volume. Gray and white matter volumes of individuals were extracted by the Easy Volume toolbox (http://www.sbirc.ed.ac.uk/LCL/LCL_M1.html) [23] running on Matlab 7.0.

DEX/CRH Test

The DEX/CRH test was administered by a single examiner (H.H.) according to a simple protocol [24], which was modified from the original protocol of Heuser et al. [25]. This simple protocol was described in our previous reports [26, 27]. The subjects took 1.5 mg of DEX (Banyu Pharmaceutical Corp., Tokyo, Japan) orally at 23:00 h. Compliance was monitored at the time of blood collection by asking them whether they had taken the tablet as directed on the previous night. On the next day, they attended our laboratory and sat on a comfortable couch in a calm room. A vein was cannulated at 14:30 h to collect blood at 15:00 and 16:00 h via an intravenous catheter. Human CRH (100 mg; hCRH 'Mitsubishi'; Mitsubishi Pharma Corp., Tokyo, Japan) was administered intravenously at 15:00 h, immediately after the first blood collection. Blood samples were immediately centrifuged and stored at −20°C. The plasma concentration of cortisol was measured by radioimmunoassay at SRL Inc. (Tokyo, Japan). The detection limit for cortisol was 1.0 μg/dl. A cortisol value under the detection limit was treated as 0 mg/dl. For cortisol, the intra-assay coefficients of variation at 2.37, 13.02 and 36.73 mg/dl were 6.90, 4.94 and 5.78%, respectively. The interassay coefficients of variation at 2.55, 13.04 and 34.17 mg/dl were 8.91, 6.03 and 6.44%, respectively (SRL Inc.).

Table 1. Cortisol levels of subjects in DEX/CRH test

	DEX/CRH test sample, μg/dl (n = 34)
15:00 h (CL-1)	0.5±0.7
16:00 h (CL-2)	6.0±5.4

Values are means ± SD. CL = Cortisol level.

Statistical Analysis

Statistical analyses were performed using the SPM8 software. Correlations of regional gray matter volume, FA and MD value maps with plasma cortisol concentrations derived from the DEX/CRH test were assessed using age and whole brain volume as nuisance variables in the study of gray matter volume, and age as a nuisance variable in the study of DTI metrics. Only correlations that met these criteria were deemed statistically significant. In this case, a seed level of $p < 0.001$ (uncorrected) and a cluster level of $p < 0.05$ (uncorrected) were used.

Results

Mean cortisol levels in the DEX/CRH test are shown in table 1. There was no significant correlation of age with cortisol levels at 15:00 h (CL-1) or those at 16:00 h (CL-2; Pearson's correlation coefficient of 0.15, $p = 0.39$, for CL-1, and of 0.23, $p = 0.20$, for CL-2). CL-1 were under the

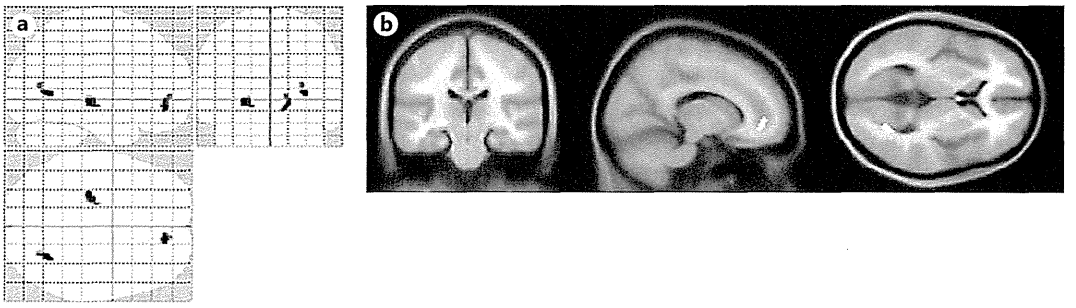

Fig. 2. There was a negative correlation between cortisol level at 16:00 h in the DEX/CRH test (**a**) and FA values in the right anterior cingulate, left parahippocampal region and right occipital region (**b**). $p < 0.001$, uncorrected.

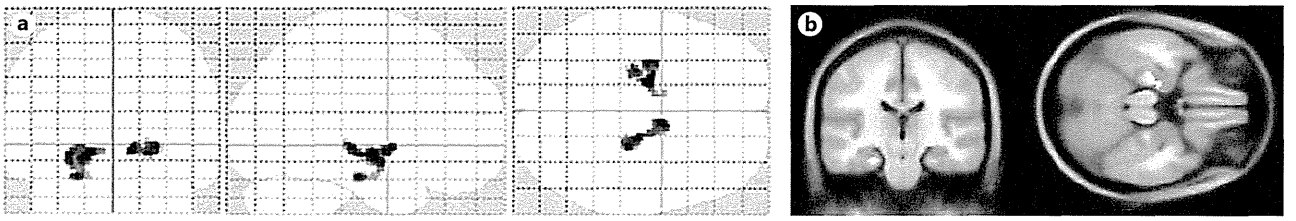

Fig. 3. There was a positive correlation between cortisol level at 16:00 h in the DEX/CRH test (**a**) and MD values in left hippocampus and bilateral parahippocampal regions (**b**). $p < 0.001$, uncorrected.

Table 2. Regions of statistically significant negative correlation between FA value and CL-2 using age as a nuisance variable

Cluster size	Z score	x	y	z	Brain region
55	4.25	−26	−24	−4	left parahippocampal region
42	3.99	28	−70	10	right occipital region
40	3.91	14	44	−8	anterior cingulum

Table 3. Regions of statistically significant positive correlation between MD value and CL-2 using age as a nuisance variable

Cluster size	Z score	x	y	z	Brain region
202	3.89	−24	−20	−22	left hippocampus
	3.97	−28	−12	−8	left parahippocampal region
120	3.96	20	−18	−8	right parahippocampal region
	3.92	26	−26	−4	right parahippocampal region

detection limit (1.0 μg/dl) in 24 out of 34 subjects, and CL-1 had no significant correlation with brain morphology (data not shown). As regards CL-2, i.e. cortisol levels after the CRH challenge, only 1 subject had levels under the detection limit. There were nominally significant negative correlations between CL-2 and gray matter volumes in the right occipital and left parahippocampal regions (fig. 1; seed level: $p < 0.01$; voxel size: >200, uncorrected), but they did not reach statistical significance ($p < 0.001$).

There was a significantly negative correlation between FA value and CL-2 in the right anterior cingulate, left parahippocampal region and right occipital region (fig. 2; table 2). There were significantly positive correlations between MD value and CL-2 in the left hippocampus and bilateral parahippocampal regions (fig. 3; table 3).

Discussion

We found that there were significant correlations between cortisol levels 1 h after the CRH injection in the DEX/CRH test and brain images in many regions

throughout the brain such as the anterior cingulate, hippocampus and the parahippocampal region. To our knowledge, this is the first study that examined the association of HPA axis activity as measured by the DEX/CRH test with brain morphology using a whole brain DTI scan. Some previous studies examined the relationships of cortisol level to the hippocampus [7, 15, 28–31], the anterior cingulate [10, 15], the ventricle [32] and the temporal region [9]; however, results were inconsistent. Some studies showed negative correlations between hippocampal volume and HPA axis activity [7, 31], but others did not [9, 15, 28–30]. As for the temporal gyrus, one study found a significantly negative correlation between its volume and HPA axis activity [9], but another study showed no such correlation [7]. With respect to the cingulum, one study reported a negative correlation between HPA axis activity and volume of the anterior cingulate [10]. One study stated that there was no correlation between HPA axis activity and volume of the ventricle [32]. Some studies showed relationships between HPA axis activity and left/right ratio of the DTI metrics in the hippocampus and cingulum [15, 16]. On the other hand, there have been a few studies that examined the possible association of an impaired feedback system of the HPA axis with whole brain configuration. One study examined the association using the VBM method; however, no remarkable findings were obtained [33]. Another study showed a positive correlation between HPA axis activity and hippocampal gray matter volume in healthy young adults [34]. Although the results of Narita et al. [34] are contrary to those of the abovementioned previous studies, the authors excluded subjects who showed HPA axis hyperactivity; therefore, whether there was an association between hyperactivity of the HPA axis and hippocampal atrophy is unknown.

We found that CL-2 in the DEX/CRH test correlated with morphological changes in many brain areas. Cortisol has a variety of effects, including suppression of inflammation and immune reactions, as well as inhibition of the secretion of several hormones and neuropeptides, which may lead to disruption of synaptic plasticity, impairing neurogenesis and causing atrophy of dendritic processes and, in an extreme case, neuronal death [35–37]. Regulation of HPA axis activity is thought to be determined by genetic [38, 39] and environmental factors such as intrauterine/early postnatal insults [40]. The long-term cortisol hypersecretion regulated by the HPA axis is therefore likely to influence brain morphology. Cortisol is known to affect cellular glucose metabolism and decrease glucose utilization in the brain, and a fluorodeoxyglucose positron emission tomography study showed a generalized reduction in cerebral glucose metabolism in all areas of the brain in patients with Cushing's disease [41]. A previous MRI volume study showed that individuals with Cushing's disease had diffuse cerebral atrophy [42]. Although almost all previous studies [7, 10, 28–32] focused on specific brain regions rich in glucocorticoid receptors, such as the hippocampus and the anterior cingulate, it should be more informative to examine a possible relation of cortisol level to regions throughout the brain. Our results showed that HPA axis activity was related to many areas of the brain. Among them, we found positive correlations between MD in the hippocampus and parahippocampi and CL-2, and a negative correlation was also observed between FA and CL-2 in the anterior cingulate and parahippocampus. The hippocampus is not only a target for cortisol but is also involved in the regulation of the HPA axis [2, 43]. Lesions to the hippocampus are associated with an increased basal cortisol level [44], and the hippocampus has been implicated in regulating cortisol release during stress [45]. Thus, the hippocampal atrophy could be both a result of, and a contributory cause of, the elevated basal cortisol level. The anterior cingulate, which also modulates the HPA axis [10], may not only be a target for cortisol but also be involved in its regulation as well. The slight discrepancy between the results of MD and FA may be due to the fact that spatial normalization of subcortical white matter is less effective, and the heterogeneous FA map more than the relatively uniform MD map cannot be normalized well [46, 47]. We found a significant association between HPA axis activity and bilateral parahippocampal regions in MD, but not in FA, values. Since parahippocampal regions comprise fibers connecting heteromodally, there might be no intense anisotropy. For the evaluation of brain microstructure in the regions where some fiber tracts ran through, MD, i.e. the mean eigenvalue of each direction, is more suitable than FA, i.e. the anisotropy along only the direction of the largest eigenvalue.

The findings reported here should be interpreted in the context of a number of limitations. First, the sample size was relatively small, which may have led to type II errors. Further work with larger sample sizes may elucidate more brain regions associated with HPA axis activity. Secondly, we included only healthy women, and the findings cannot be generalized to men. Thirdly, we only made a linear correlational analysis; thus, even if there were a U-shaped relationship between the HPA axis and brain morphology, such a relationship could not be detected.

Our data suggest that an increased cortisol level after the DEX/CRH test is related to morphological changes in a variety of brain regions. Especially, local microstructural characteristics or neural connectivity estimated by DTI in the hippocampus, the parahippocampal regions and the cingulate cortices, i.e. regions in which glucocorticoid receptors are abundantly distributed [48], were suggested to be correlated with hyperactivity in the HPA axis.

Acknowledgement

This study was supported by Health and Labor Sciences Research Grants (Comprehensive Research on Disability, Health and Welfare), an Intramural Research Grant (24-11) for Neurological and Psychiatric Disorders from the National Center of Neurology and Psychiatry (M.O. and H.K.), and 'Understanding of molecular and environmental bases for brain health' carried out under the Strategic Research Program for Brain Sciences by the Ministry of Education, Culture, Sports, Science and Technology of Japan (H.K.).

References

1 McEwen BS: Protective and damaging effects of stress mediators. N Engl J Med 1998;338:171–179.

2 Jacobson L, Sapolsky RM: The role of the hippocampus in feedback regulation of the hypothalamic-pituitary-adrenal axis. Endocr Rev 1991;12:118–134.

3 Armanini MP, Hutchins C, Stein BA, Sapolsky RM: Glucocorticoid endangerment of hippocampal neurons is NMDA-receptor dependent. Brain Res 1990;532:7–12.

4 Patel R, McIntosh L, McLaughlin J, Brooke S, Nimon V, Sapolsky R: Disruptive effects of glucocorticoids on glutathione peroxidase biochemistry in hippocampal cultures. J Neurochem 2002;82:118–125.

5 Nair SM, Werkman TR, Craig J, Finnell R, Joëls M, Eberwine JH: Corticosteroid regulation of ion channel conductances and mRNA levels in individual hippocampal CA1 neurons. J Neurosci 1998;18:2685–2696.

6 Holsboer F, von Bardeleben U, Wiedemann K, Müller OA, Stalla GK: Serial assessment of corticotropin-releasing hormone response after dexamethasone in depression: implications for pathophysiology of DST nonsuppression. Biol Psychiatry 1987;22:228–234.

7 Lupien SJ, de Leon M, de Santi S, Convit A, Tarshish C, Thakur M, McEwen BS, Hauger RL, Meaney MJ: Cortisol levels during human aging predict hippocampal atrophy and memory deficits. Nat Neurosci 1998;1:69–73.

8 Wolf OT, Convit A, de Leon MJ, Caraos C, Qadri SF: Basal hypothalamo-pituitary-adrenal axis activity and corticotropin feedback in young and older men: relationships to magnetic resonance imaging-derived hippocampus and cingulate gyrus volumes. Neuroendocrinology 2002;75:241–249.

9 MacLullich AM, Deary IJ, Starr JM, Ferguson KJ, Wardlaw JM, Seckl JR: Plasma cortisol levels, brain volumes and cognition in healthy elderly men. Psychoneuroendocrinology 2005;30:505–515.

10 MacLullich AM, Ferguson KJ, Wardlaw JM, Starr JM, Deary IJ, Seckl JR: Smaller left anterior cingulate cortex volumes are associated with impaired hypothalamic-pituitary-adrenal axis regulation in healthy elderly men. J Clin Endocrinol Metab 2006;91:1591–1594.

11 Gold SM, Dziobek I, Rogers K, Bayoumy A, McHugh PF, Convit A: Hypertension and hypothalamo-pituitary-adrenal axis hyperactivity affect frontal lobe integrity. J Clin Endocrinol Metab 2005;90:3262–3267.

12 Meaney MJ, Aitken DH: [^{3}H]Dexamethasone binding in rat frontal cortex. Brain Res 1985;328:176–180.

13 Basser PJ, Pierpaoli C: Microstructural and physiological features of tissue elucidated by quantitative diffusion-tensor MRI. J Magn Reson B 1996;111:209–219.

14 Pierpaoli C, Basser PJ: Toward a quantitative assessment of diffusion anisotropy. Magn Reson Med 1996;36:893–906.

15 Madsen KS, Jernigan TL, Iversen P, Frokjaer VG, Knudsen GM, Siebner HR, Baaré WF: Hypothalamic-pituitary-adrenal axis tonus is associated with hippocampal microstructural asymmetry. Neuroimage 2012;63:95–103.

16 Madsen KS, Jernigan TL, Iversen P, Frokjaer VG, Mortensen EL, Knudsen GM, Baaré WF: Cortisol awakening response and negative emotionality linked to asymmetry in major limbic fibre bundle architecture. Psychiatry Res 2012;201:63–72.

17 Otsubo T, Tanaka K, Koda R, Shinoda J, Sano N, Tanaka S, Aoyama H, Mimura M, Kamijima K: Reliability and validity of Japanese version of the Mini-International Neuropsychiatric Interview. Psychiatry Clin Neurosci 2005;59:517–526.

18 Sheehan DV, Lecrubier Y, Sheehan KH, Amorim P, Janavs J, Weiller E, Hergueta T, Baker R, Dunbar GC: The Mini-International Neuropsychiatric Interview (MINI): the development and validation of a structured diagnostic psychiatric interview for DSM-IV and ICD-10. J Clin Psychiatry 1998;59:22–57.

19 Ashburner J: A fast diffeomorphic image registration algorithm. Neuroimage 2007;38:95–113.

20 Yassa MA, Stark CE: A quantitative evaluation of cross-participant registration techniques for MRI studies of the medial temporal lobe. Neuroimage 2009;44:319–327.

21 Smith SM, Nichols TE: Threshold-free cluster enhancement: addressing problems of smoothing, threshold dependence and localisation in cluster inference. Neuroimage 2009;44:83–98.

22 Jones DK, Cercignani M: Twenty-five pitfalls in the analysis of diffusion MRI data. NMR Biomed 2010;23:803–820.

23 Pernet C, Andersson J, Paulesu E, Demonet JF: When all hypotheses are right: a multifocal account of dyslexia. Hum Brain Mapp 2009;30:2278–2292.

24 Kunugi H, Ida I, Owashi T, Kimura M, Inoue Y, Nakagawa S, Yabana T, Urushibara T, Kanai R, Aihara M, Yuuki N, Otsubo T, Oshima A, Kudo K, Inoue T, Kitaichi Y, Shirakawa O, Isogawa K, Nagayama H, Kamijima K, Nanko S, Kanba S, Higuchi T, Mikuni M: Assessment of the dexamethasone/CRH test as a state-dependent marker for hypothalamic-pituitary-adrenal (HPA) axis abnormalities in major depressive episode: a multicenter study. Neuropsychopharmacology 2006;31:212–220.

25 Heuser I, Yassouridis A, Holsboer F: The combined dexamethasone/CRH test: a refined laboratory test for psychiatric disorders. J Psychiatr Res 1994;28:341–356.

26 Hori H, Ozeki Y, Teraishi T, Matsuo J, Kawamoto Y, Kinoshita Y, Suto S, Terada S, Higuchi T, Kunugi H: Relationships between psychological distress, coping styles, and HPA axis reactivity in healthy adults. J Psychiatr Res 2010;44:865–873.

27 Hori H, Teraishi T, Ozeki Y, Hattori K, Sasayama D, Matsuo J, Kawamoto Y, Kinoshita Y, Higuchi T, Kunugi H: Schizotypal personality in healthy adults is related to blunted cortisol responses to the combined dexamethasone/corticotropin-releasing hormone test. Neuropsychobiology 2011;63:232–241.

28 Axelson DA, Doraiswamy PM, McDonald WM, Boyko OB, Tupler LA, Patterson LJ, Nemeroff CB, Ellinwood EH Jr, Krishnan KR: Hypercortisolemia and hippocampal changes in depression. Psychiatry Res 1993;47:163–173.

29 O'Brien JT, Ames D, Schweitzer I, Colman P, Desmond P, Tress B: Clinical and magnetic resonance imaging correlates of hypothalamic-pituitary-adrenal axis function in depression and Alzheimer's disease. Br J Psychiatry 1996;168:679–687.

30 Sandström A, Peterson J, Sandström E, Lundberg M, Nystrom IR, Nyberg L, Olsson T: Cognitive deficits in relation to personality type and hypothalamic-pituitary-adrenal (HPA) axis dysfunction in women with stress-related exhaustion. Scand J Psychol 2011;52:71–82.

31 Starkman MN, Gebarski SS, Berent S, Schteingart DE: Hippocampal formation volume, memory dysfunction, and cortisol levels in patients with Cushing's syndrome. Biol Psychiatry 1992;32:756–765.

32 Risch SC, Lewine RJ, Kalin NH, Jewart RD, Risby ED, Caudle JM, Stipetic M, Turner J, Eccard MB, Pollard WE: Limbic-hypothalamic-pituitary-adrenal axis activity and ventricular-to-brain ratio studies in affective illness and schizophrenia. Neuropsychopharmacology 1992;6:95–100.

33 Rydmark I, Wahlberg K, Ghatan PH, Modell S, Nygren A, Ingvar M, Asberg M, Heilig M: Neuroendocrine, cognitive and structural imaging characteristics of women on longterm sickleave with job stress-induced depression. Biol Psychiatry 2006;60:867–873.

34 Narita K, Fujihara K, Takei Y, Suda M, Aoyama Y, Uehara T, Majima T, Kosaka H, Amanuma M, Fukuda M, Mikuni M: Associations among parenting experiences during childhood and adolescence, hypothalamus-pituitary-adrenal axis hypoactivity, and hippocampal gray matter volume reduction in young adults. Hum Brain Mapp 2011;33:2211–2223.

35 Munck A, Guyre P, Holbrook N: Physiological functions of glucocorticoids in stress and their relation to pharmacological actions. Endocr Rev 1984;5:25–42.

36 Sapolsky RM: Glucocorticoids and hippocampal atrophy in neuropsychiatric disorders. Arch Gen Psychiatry 2000;57:925–935.

37 Sapolsky R, Romero L, Munck A: How do glucocorticoids influence the stress-response? Integrating permissive, suppressive, stimulatory, and preparative actions. Endocr Rev 2000;21:55–73.

38 Bartels M, van den Berg M, Sluyter F, Boomsma DI, de Geus EJC: Heritability of cortisol levels: review and simultaneous analysis of twin studies. Psychoneuroendocrinology 2003;28:121–137.

39 Sasayama D, Hori H, Iijima Y, Teraishi T, Hattori K, Ota M, Fujii T, Higuchi T, Amano N, Kunugi H: Modulation of cortisol responses to the DEX/CRH test by polymorphisms of the interleukin-1beta gene in healthy adults. Behav Brain Funct 2011;7:23.

40 Welberg LAM, Seckl JR: Prenatal stress, glucocorticoids and the programming of the brain. J Neuroendocrinol 2001;13:113–128.

41 Brunetti A, Fulham MJ, Aloj L, de Souza B, Nieman L, Oldfield EH, di Chiro G: Decreased brain glucose utilization in patients with Cushing's disease. J Nucl Med 1998;39:786–790.

42 Bourdeau I, Bard C, Noël B, Leclerc I, Cordeau MP, Bélair M, Lesage J, Lafontaine L, Lacroix A: Loss of brain volume in endogenous Cushing's syndrome and its reversibility after correction of hypercortisolism. J Clin Endocrinol Metab 2002;87:1949–1954.

43 Sapolsky RM: Stress, the Aging Brain, and the Mechanisms of Neuron Death. Cambridge, MIT Press, 1992.

44 Fischette CT, Komisaruk BR, Edinger HM, Feder HH, Siegel A: Differential fornix ablations and the circadian rhythmicity of adrenal corticosteroid secretion. Brain Res 1980;195:373–387.

45 de Kloet ER: Brain corticosteroid receptor balance and homeostatic control. Front Neuroendocrinol 1991;12:95–164.

46 Eriksson SH, Rugg-Gunn FJ, Symms MR, Barker GJ, Duncan JS: Diffusion tensor imaging in patients with epilepsy and malformations of cortical development. Brain 2001;124:617–626.

47 Snook L, Plewes C, Beaulieu C: Voxel based versus region of interest analysis in diffusion tensor imaging of neurodevelopment. Neuroimage 2007;34:243–252.

48 Mizoguchi K, Ishige A, Aburada M, Tabira T: Chronic stress attenuates glucocorticoid negative feedback: involvement of the prefrontal cortex and hippocampus. Neuroscience 2003;119:887–897.

NeuroImage: Clinical 2 (2013) 491–496

Contents lists available at ScienceDirect

NeuroImage: Clinical

journal homepage: www.elsevier.com/locate/ynicl

In vivo evaluation of gray and white matter volume loss in the parkinsonian variant of multiple system atrophy using SPM8 plus DARTEL for VBM☆

Yoko Shigemoto [a], Hiroshi Matsuda [b,*], Kouhei Kamiya [a], Norihide Maikusa [b], Yasuhiro Nakata [a], Kimiteru Ito [a], Miho Ota [c], Naofumi Matsunaga [d], Noriko Sato [a]

[a] Department of Radiology, National Center Hospital of Neurology and Psychiatry, 4-1-1 Ogawahigashi, Kodaira, Tokyo 187-8551 Japan
[b] Integrative Brain Imaging Center, National Center of Neurology and Psychiatry, 4-1-1 Ogawahigashi, Kodaira, Tokyo 187-8551 Japan
[c] Department of Mental Disorder Research, National Institute of Neuroscience, National Center of Neurology and Psychiatry, 4-1-1 Ogawa-Higashi, Kodaira, Tokyo 187-8502, Japan
[d] Department of Radiology, Yamaguchi University Graduate School of Medicine, 1-1-1 Minamikogushi, Ube, Yamaguchi 755-8505, Japan

ARTICLE INFO

Article history:
Received 5 January 2013
Received in revised form 26 March 2013
Accepted 27 March 2013
Available online 5 April 2013

Keywords:
Multiple system atrophy with predominant parkinsonism (MSA-P)
White matter
Diffeomorphic anatomical registration through exponentiated Lie algebra (DARTEL)
Statistical parametric mapping (SPM)
Voxel-based morphometry (VBM)

ABSTRACT

In multiple system atrophy with predominant parkinsonism (MSA-P), several voxel-based morphometry (VBM) studies have revealed gray matter loss; however, the white matter volume changes have been rarely reported. We investigated the volume changes of white matter as well as gray matter by VBM. A retrospective MRI study was performed in 20 patients with MSA-P and 30 age-matched healthy controls. We applied VBM with statistical parametric mapping (SPM8) plus diffeomorphic anatomical registration through exponentiated Lie algebra (DARTEL) to explore the regional atrophy of gray and white matter in all of the MSA-P patients, 14 patients with left-side dominant and 6 patients with right-side dominant onset as compared to controls. In all of the MSA-P patients, VBM revealed a significant volume reduction of gray matter in the bilateral putamina, cerebellums and dorsal midbrain. White matter loss was located in bilateral globus pallidi, external capsules extending to the midbrain, right subcortical to precentral area through internal capsule, the pons, bilateral middle cerebellar peduncles and left cerebellum. In left-side dominant MSA-P patients, the gray and white matter volume loss was detected predominantly on the right side and vice versa in right-side dominant MSA-P patients. A correlation with disease duration and severity was not detected. VBM using SPM8 plus DARTEL detected significant volume loss not only in the gray but also in the white matter of the area affected by MSA-P.

1. Introduction

MSA is a sporadic, progressive, neurodegenerative disorder clinically characterized by autonomic dysfunction, parkinsonism, cerebellar ataxia, and pyramidal signs (Quinn, 1989). MSA can be classified into two subgroups, a cerebellar (MSA-C) and a parkinsonian (MSA-P) variant (Gilman et al., 2008). Neuropathologically, MSA is characterized by selective neuronal loss and reactive gliosis predominantly affecting the basal ganglia, substantia nigra, olivopontocerebellar pathways and the intermediolateral cell column of the spinal cord (Papp and Lantos, 1994; Wenning et al., 1997). The histological hallmarks of MSA are α-synuclein-positive glial cytoplasmic inclusions in the oligodendroglia, which are required for the diagnosis of definite MSA (Gilman et al., 2008; Papp and Lantos, 1994; Wenning et al., 1997).

VBM is a method of statistically analyzing morphological changes in the brain as measured by whole-brain MRI data (Ashburner and Friston, 2000). In the past few years, VBM has been used to study the patterns of structural changes in the brain during brain development or in neurodegenerative disorders (Bergfield et al., 2010; Brenneis et al., 2004; Burton et al., 2002). In MSA-P, VBM revealed gray matter loss mainly in the striatum, the cerebral cortex including the motor area and the cerebellar lobes (Brenneis et al., 2003, 2007; Minnerop et al., 2007; Tir et al., 2009; Tzarouchi et al., 2010). However, white matter volume changes have been rarely reported, and the results were inconsistent (Brenneis et al., 2003; Minnerop et al., 2007, 2010; Tzarouchi et al., 2010).

In the present study, we evaluated MR images of MSA-P patients to examine the volume changes of white matter as well as gray matter by using the latest VBM technique with SPM 8 plus DARTEL (Matsuda et al., 2012).

* Corresponding author at: 4-1-1 Ogawahigashi, Kodaira, Tokyo 187-8551, Japan. Tel.: +81 42 341 2712x2171; fax: +81 42 346 2229.
E-mail address: matsudah@ncnp.go.jp (H. Matsuda).

2213-1582/$ – see front matter © 2013 The Authors. Published by Elsevier Inc. All rights reserved.
http://dx.doi.org/10.1016/j.nicl.2013.03.017

2. Materials and methods

2.1. Participants

We retrospectively reviewed an electronic database of radiology reports for 12,029 patients who underwent brain MRI examinations at our institution between March 2007 and September 2010 and searched for reports that indicated Parkinson's disease and related disorders. After 127 patients were indicated by the radiological reports, medical records revealed 23 patients who were diagnosed as possible or probable MSA-P according to consensus criteria (Gilman et al., 2008). Among 23 patients, three patients were excluded because of the presence of multiple lacunar infarctions in two patients and multiple cavernous hemangiomas in one patient. All volumetric T1-weighted images were visually inspected for apparent artifacts due to patient motion or metallic dental prostheses. As a consequence, 20 patients (7 men and 13 women; age range 48–77 years, mean age 62.9 ± 7.7 years, disease duration 4.1 ± 2.2 years) were enrolled as subjects in this study. The patient data are given in Table 1. Among these patients, 14 patients had left-side dominant (5 men and 9 women; age range 53–77 years, mean age 64.1 ± 6.4 years, disease duration 4.2 ± 2.5 years) and 6 patients had right-side dominant onset symptoms (2 men and 4 women; age range 48–73 years, mean age 59.8 ± 10.0 years, disease duration 3.7 ± 1.2 years). As a measure of disease severity, we adopted the following disease stages previously described: stage 0 = no gait difficulties, stage 1 = disease onset, as defined by onset of gait difficulties, stage 2 = loss of independent gait, as defined by permanent use of a walking aid or reliance on a supporting arm, stage 3 = confinement to wheelchair, as defined by permanent use of a wheelchair (Klockgether et al., 1998).

Our local ethics committee did not require approval or patient informed consent for the retrospective review. Thirty age-matched control subjects (10 men and 20 women; age range 48–80 years, mean age 64.7 ± 7.7 years) were also involved as healthy control subjects.

Thirty age-matched healthy controls (10 men and 20 women; age range 48–80 years, mean age 64.7 ± 7.7 years) were also involved as control subjects. None had a history of neurological or psychiatric illness, and no abnormalities were observed on their brain structural MRIs. Institutional review board approval and written informed consent were obtained from the control subjects.

2.2. Image acquisition and analysis

All examinations were performed with a 1.5 T MR imaging system (Symphony Vision; Siemens, Erlangen, Germany). MR protocol for the parkinsonian is as follows. High-resolution three-dimensional (3D) T1-weighted images were acquired using magnetization-prepared rapid acquisition of a gradient echo sequence (144 sagittal sections, TR = 1600 ms, TE = 2.6 ms, flip angle = 15°, voxel size = 1.2 × 1.2 × 1.2 mm^3, FOV = 315 mm, matrix = 208 × 256, 1.2-mm thickness with no gap). Axial T2-weighted images (TR = 3800 ms, TE = 95 ms, flip angle = 150°, voxel size = 0.7 × 0.4 × 5.0 mm^3, FOV = 230 mm, matrix = 281 × 512, 5-mm thickness with 1.8-mm gap) and coronal fluid attenuation inversion recovery images (TR = 9000 ms, TE = 100 ms, flip angle = 170°, voxel size = 1.2 × 0.9 × 5.0 mm^3, FOV 230 mm, matrix = 192 × 256, 5.0-mm thickness with 1.8-mm gap) were also obtained.

Using the latest version of SPM8 (Wellcome Department of Imaging Neuroscience, London, United Kingdom), we segmented the MRIs into gray matter, white matter, and cerebrospinal fluid images by a unified tissue-segmentation procedure after image-intensity nonuniformity correction. These segmented gray and white matter images were then spatially normalized to the customized template in the standardized anatomic space by using DARTEL (Wellcome Department of Imaging Neuroscience) (Ashburner, 2007). To preserve the gray and white matter volumes within each voxel, we modulated the images using the Jacobean determinants derived from the spatial normalization by DARTEL and then smoothed them using an 8-mm FWHM Gaussian kernel.

Morphological group differences for these smoothed gray and white matter images between all of the MSA-P patients and the controls were analyzed using a 2-sample *t*-test in SPM8. The same analysis was performed between the 14 left-side dominant onset MSA-P patients and the controls and between the 6 right-side dominant onset MSA-P patients and the controls. Group comparisons by SPM8 were assessed using the false discovery rate at a threshold of $p < .05$, corrected for multiple comparisons.

Additionally, for the correlation analyses with disease duration and disease stage, we used a multiple regression analysis and an uncorrected threshold of $p < .001$.

3. Results

In MSA-P patients, VBM revealed regions of gray matter loss bilaterally affecting the putamina, cerebellums, dorsal midbrain and left inferior occipital gyrus (see Table 2, Fig. 1). Reduced white matter volume was located in the bilateral globus pallidi and external capsules extending to the midbrain (see Table 3, Fig. 2). On the right side, it extended upward to the subcortical to precentral area through the internal capsule. White matter loss in the pons, bilateral middle cerebellar peduncles and left cerebellum was also detected. In left-side dominant MSA-P patients, the putaminal gray matter was decreased only on the right side (see Table 4, Fig. 3). The reduced white matter was located in the right globus pallidus and external capsule (see Table 5, Fig. 3). In right-side dominant MSA-P patients, gray matter was reduced in the left putamen, bilateral cerebellums

Table 1
Demographic characteristics of MSA-P patients and controls.

Characteristic	MSA-P	Controls
Age (y)	62.9 ± 7.7 (48–77)	62.9 ± 7.7 (48–80)
Sex	7 men, 13 women	10 men, 20 women
Diagnosis	16 probable MSA-P, 4 possible MSA-P	
Disease duration (y)	4.1 ± 2.2 (2–10)	
Stage 1	6	
Stage 2	11	
Stage 3	3	
Cerebellar symptoms	7 present, 13 absent	
Pyramidal signs	7 present, 13 absent	
Urinary incontinence	15 present, 5 absent	
Orthostatic hypotension	13 present, 7 absent	

Note: Unless otherwise indicated, data are means ± standard deviations, with ranges in parentheses. Stage 0 = no gait difficulties, stage 1 = disease onset, as defined by onset of gait difficulties, stage 2 = loss of independent gait, as defined by permanent use of a walking aid or reliance on a supporting arm, stage 3 = confinement to wheelchair, as defined by permanent use of a wheelchair.

Table 2
Clusters of gray matter loss (20 MSA-P vs. 30 controls).

Region volume (mm^3)	Z score	Talairach coordinates (x, y, z)	Location of local maxima
9680	4.46	40, −46, −36	Right cerebellar tonsil
	3.79	36, −69, −15	Right cerebellum
	3.55	24, −46, −13	Right cerebellum
8424	6.36	26, 14, 7	Right putamen
6960	4.31	−40, −54, −23	Left cerebellum
	3.6	−28, −84, −9	Left inferior occipital gyrus
	3.31	−20, −75, −20	Left cerebellum
5712	6.05	−26, 8, 7	Left putamen
3896	4.6	0, −34, −12	Dorsal midbrain

Voxel size 2 × 2 × 2 mm^3. Clusters of gray matter SPM analysis with FDR-corrected at $p < .05$ are shown. The coordinates refer to the Talairach reference space.

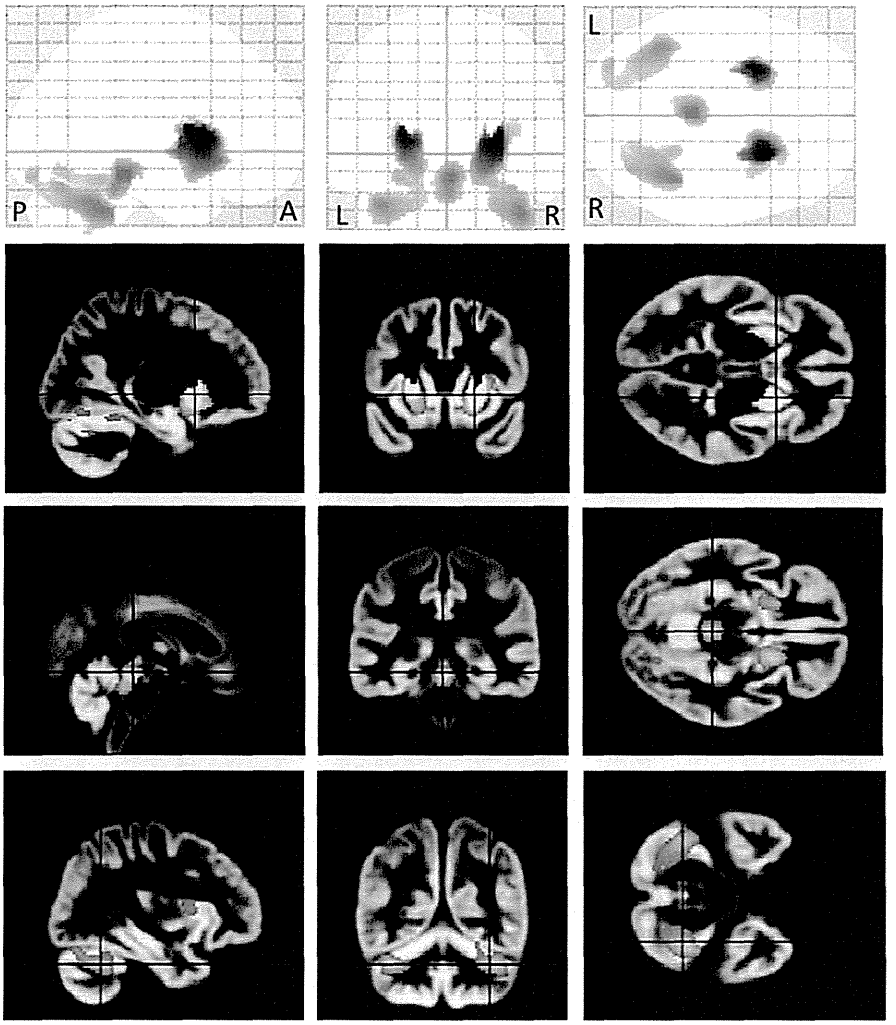

Fig. 1. Comparison of gray matter volume by VBM using SPM8 plus DARTEL among 20 patients with MSA-P and 30 control subjects. Significant atrophy is observed in the bilateral putamina, cerebellums, dorsal midbrain and left inferior occipital gyrus in MSA-P patients compared to controls. Results are superimposed on the customized gray matter template (FDR-corrected at $p < .05$).

and several cortical regions (see Table 6, Fig. 4). The reduced white matter was located in the left globus pallidus, bilateral external capsules, right frontal lobe, right parahippocampal area and right cerebellum (see Table 7, Fig. 4). A correlation with disease duration and severity was not detected.

Table 3
Clusters of white matter loss (20 MSA-P vs. 30 controls).

Region volume (mm^3)	Z score	Talairach coordinates (x, y, z)	Location of local maxima
32,144	4.23	−12, −64, −34	Left cerebellum
	4.12	−16, −27, −32	Left pons
	4.07	−16, −38, −22	Left cerebellum
20,360	5.46	32, −10, 2	Right external capsule
	4.94	18, 2, −5	Right lateral globus pallidus
	3.35	36, −6, 32	Right sub-precentral area
10,272	5.04	−34, −8, 4	Left external capsule
	4.79	−20, −2, −5	Left lateral globus pallidus

Voxel size 2 × 2 × 2 mm^3. Clusters of gray matter SPM analysis with FDR-corrected at $p < .05$ are shown. The coordinates refer to the Talairach reference space.

4. Discussion

To our knowledge, this is the first study to focus on the white matter volume loss in MSA-P patients as determined by VBM using SPM8 plus DARTEL. This analysis showed white matter atrophy in the globus pallidi and external capsules bilaterally extending to the midbrain. The white matter atrophy also spreads upward to the subcortical to right premotor area. These areas correspond to the regions connecting the pathologically affected structures. Such findings, which seemed to reflect the degeneration of the motor pathway, have never been presented in previous VBM studies. We believe that the evaluation of white matter as well as deep gray matter has significantly improved owing to this new software.

Neuropathological studies have shown neuronal loss and reactive gliosis in the putamen, caudate nucleus, external pallidum, substantia nigra, locus coeruleus, inferior olives, pontine nuclei, cerebellar lobes and intermediolateral cell columns of the spinal cord in MSA-P (Wenning et al., 1997). Most severe neuronal loss was found in the lateral part of the substantia nigra and dorsolateral putamen (Jellinger et al., 2005; Ozawa et al., 2004; Wenning et al., 2002). The previous VBM studies have reported gray matter loss in the putamen, caudate nucleus,

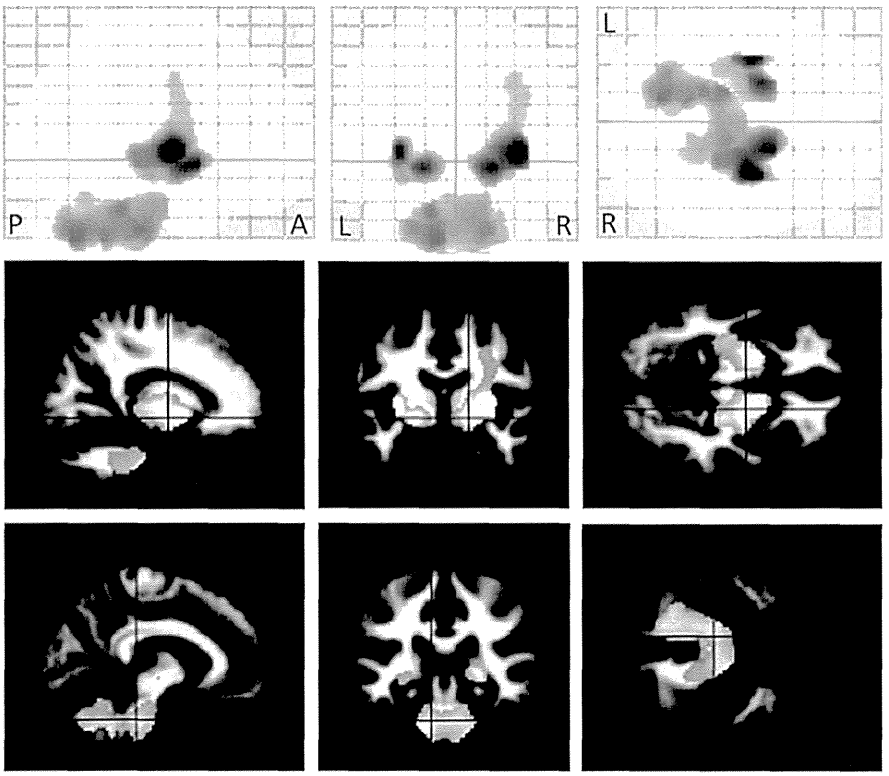

Fig. 2. Comparison of white matter volume by VBM using SPM8 plus DARTEL among 20 patients with MSA-P and 30 control subjects. Significant atrophy is observed in the bilateral globus pallidi and external capsules extending to the midbrain. On the right side, the atrophy extends upward to the subcortical to precentral area through the internal capsule. White matter atrophy in the pons, bilateral middle cerebellar peduncles and left cerebellum is also detected. Results are superimposed on the customized white matter template (FDR-corrected at $p < .05$).

Table 4
Clusters of gray matter loss (14 left-side dominant onset MSA-P vs. 30 controls).

Region volume (mm^3)	Z score	Talairach coordinates (x, y, z)	Location of local maxima
6864	6.38	26, 14, 5	Right putamen

Voxel size $2 \times 2 \times 2$ mm^3. Clusters of gray matter SPM analysis with FDR-corrected at $p < .05$ are shown. The coordinates refer to the Talairach reference space.

cerebellar vermis and lobes, dorsal midbrain, and several cortical regions including the insular cortex and motor area (Brenneis et al., 2003, 2007; Chang et al., 2009; Minnerop et al., 2007, 2010; Tir et al., 2009; Tzarouchi et al., 2010). The significant putaminal loss detected in our study confirmed the findings of previous region of interest based morphometric and VBM studies (Brenneis et al., 2003, 2007; Minnerop et al., 2007; Schulz et al., 1999; Tzarouchi et al., 2010). Our VBM results also agree with the pathological features (Jellinger et al., 2005; Ozawa et al., 2004; Wenning et al., 1997, 2002).

Though some previous VBM studies have detected the atrophy of the caudate nucleus (Brenneis et al., 2003; Chang et al., 2009; Tzarouchi et al., 2010), our study did not detect volume loss in the caudate nucleus. Pathologically, the caudate nucleus is less involved than the putamen and tends to be relatively preserved in the early stage of MSA-P (Ozawa et al., 2004; Wenning et al., 2002). (Chang et al., 2009) reported that the caudate nucleus had significant atrophy compared to the putamen, a finding that is inconsistent with pathological features mentioned above. It is possible that the localization of deep gray matter at the periventricular space made it difficult to segment the MRIs in older versions of SPM. The recent report of Messina et al. (2011) supported our finding of no significant volume loss in the caudate nucleus as measured automatically by FreeSurfer.

Gray matter volume loss in the olivopontocerebellar system can also be seen in MSA-P, although the degree of involvement is lower

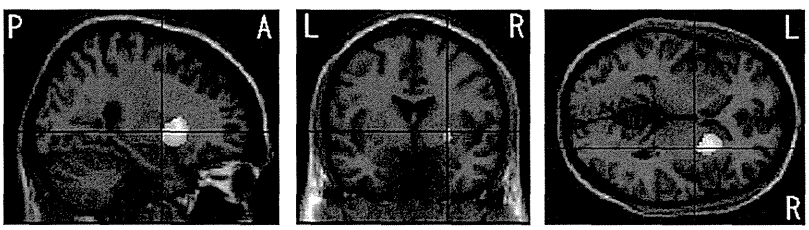

Fig. 3. Comparison of gray and white matter volumes by VBM using SPM8 plus DARTEL among 14 patients with left-side dominant onset MSA-P and 30 control subjects. Significant gray matter atrophy which is shown in a yellow color is observed only on the right side of the putamen (FDR-corrected at $p < .05$). Significant white matter atrophy which is shown in a red color is observed only on the right side of the globus pallidus and external capsule (FDR-corrected at $p < .05$).